Evidence for Holocene palaeoseismicity along the Basel-Reinach active normal fault (Switzerland): a seismic source for the 1356 earthquake in the Upper Rhine graben

M. Ferry, M. Meghraoui, B. Delouis, D. Giardini

Geophys. J. Int. (2005) **160,** 554–572 doi: 10.1111/j.1365-246X.2005.02404.x

Evidence for Holocene palaeoseismicity along the Basel–Reinach active normal fault (Switzerland): a seismic source for the 1356 earthquake in the Upper Rhine graben

Matthieu Ferry,[1] Mustapha Meghraoui,[2] Bertrand Delouis[1,*] and Domenico Giardini[1]

[1] *Institut für Geophysik, ETH-Hönggerberg,* 8093 *Zurich, Switzerland. E-mail: matthieu.ferry@sed.ethz.ch*
[2] *EOST-IPGS, UMR* 7516, 5 *rue René Descartes,* 67084 *Strasbourg, France*

Accepted 2004 May 25. Received 2004 May 25; in original form 2003 March 10

SUMMARY

We conducted a palaeoseismic study with geomorphologic mapping, geophysical prospecting and trenching along an 8-km-long NNE–SSW trending fault scarp south of Basel. The city as well as 40 castles within a 20-km radius were destroyed or heavily damaged by the earthquake of 1356 October 18 (Io = IX-X), the largest historical seismic event in central Europe. Active river incisions as well as late Quaternary alluvial terraces are uplifted along the linear Basel–Reinach (BR) fault scarp. The active normal fault is comprised of at least two main branches reaching the surface as evident by resistivity profiles, reflection seismic data and direct observations in six trenches. In trenches, the normal fault rupture affects three colluvial wedge deposits up to the base of the modern soil. Radiocarbon as well as thermoluminescence (TL) age determinations from other trenches helped to reconstruct the Holocene event chronology. We identified three seismic events with an average coseismic movement of 0.5–0.8 m and a total vertical displacement of 1.8 m in the last 7800 yr and five events in the last 13 200 yr. The most recent event occurred in the interval AD 500–1450 (2σ) and may correspond to the 1356 earthquake. Furthermore, the morphology suggests both a southern and northern fault extensions that may reach 20 km across the Jura mountains and across the Rhine valley. Taking this fault length and a 10-km-thick seismogenic layer suggests a Mw 6.5 or greater event as a possible scenario for the seismic hazard assessment of the Basel region.

Key words: active tectonics, Basel, palaeoseismicity, Upper Rhine graben.

1 INTRODUCTION

The tectonic signature of coseismic surface faulting in an active fault zone is developed and preserved as a function of rate of deformation and surface geologic processes. Successive coseismic surface rupture displacements along a fault can be studied using palaeoseismic investigations to determine a rate of the active deformation and a recurrence interval for large earthquakes. The palaeoseismic record of large or moderate earthquakes in regions with a present-day low level of seismicity has been documented to show fault slip rates much lower than 1 mm yr^{-1} and likely of the order of 0.1 mm yr^{-1} (Crone *et al.* 1997; Camelbeeck & Meghraoui 1998).

However, the identification and characterization of a seismogenic fault in these regions are major problems as a result of two main factors: (i) the rate of active deformation being quite low, surface faulting and related cumulative scarp are hardly visible unless a detailed study in active tectonics is undertaken, (ii) the surface deformation is very often hidden by either a thick vegetation cover (e.g. forests), by agricultural fields or by an urban area as it is the case along the Basel–Reinach (BR) fault. Therefore, palaeoseismic investigations across low slip rate active faults require the use of a multidisciplinary approach including geomorphology, geophysical prospecting and trenching. This approach was successfully tested along the Feldbiss fault (at Bree) in the Lower Rhine graben and the palaeoseismic results revealed the occurrence of three events with $Mw > 6.2$ in the last 30 000 yr (Meghraoui *et al.* 2000; Vanneste *et al.* 2001).

Intraplate Europe is classified among the stable continental regions because of the low rate of deformation (Fig. 1) (Johnston 1996; Camelbeeck & Meghraoui 1998). However, the historical seismicity is noteworthy and moderate to large damaging earthquakes have occurred in the past (Camelbeeck *et al.* 2000). In this context, the occurrence of the 1356 October 18 shallow earthquake in Basel is among the largest historical seismic event with maximum $Mw = 6.5$ in Western Europe (Mayer-Rosa & Cadiot 1979). This large seismic event posed the problem of the identification of the seismic source in the area of Basel (Meyer *et al.* 1994). In a previous study of the active deformation of the southern Upper Rhine graben, we have

*Now at: Géosciences Azur, Université de Nice, 06000 Nice, France.

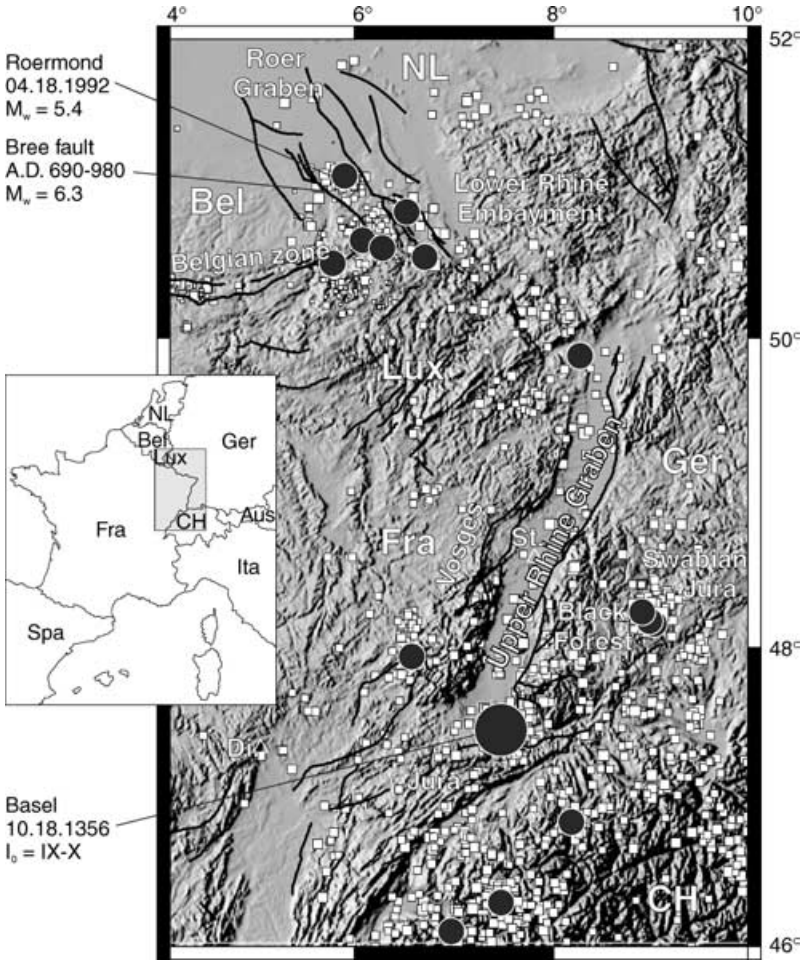

Figure 1. Seismicity and tectonics of NW Europe. Seismicity (historical in grey circles and instrumental in white squares) and Quaternary faults (black lines) of the Rhine graben underline the recent tectonic activity of intraplate Europe. Our study area is located in the vicinity of the 1356 October 18 Basel earthquake, one of the strongest seismic events in Europe (I_0 = IX-X; Mayer-Rosa & Cadiot 1979). White triangles point to Dijon (D) and Strasbourg (St) cities located more than 100 km away and that recorded strong damage to bell towers.

identified the BR active fault and shown its probable relationship with the 1356 earthquake (Meghraoui *et al.* 2001). The first results obtained from trench studies have shown the occurrence of three large seismic events with $M_w > 6$ in the last 7800 yr and a total vertical displacement of 1.8 m.

In this paper, we provide a summary of the 1356 earthquake followed by a detailed description the BR fault using the relationship between the fault scarp geomorphology (surface deformation and drainage pattern) and related distribution of late Quaternary deposits (colluvial, fluvial and alluvial terraces). Historical accounts of the 1356 seismic event are presented together with the seismotectonic and neotectonic frameworks. The surface faulting and related palaeoseismology is documented using (i) electrical resistivity profiles combined with high-resolution seismic lines and (ii) eight trenches dug across the fault at two different sites. An analysis of the long-term deformation using accelerated mass spectrometer (AMS) radiocarbon and thermoluminescence (TL) dating shows the succession of past seismic events illustrated with reconstructions and kinematical models of the surface faulting. Amounts of coseismic displacements, maximum size of the fault and recurrence interval of large earthquakes are discussed for an evaluation of the seismic hazard in the southern Upper Rhine graben.

2 THE 1356 BASEL EARTHQUAKE

On the 1356 October 18, the city of Basel was struck by a first seismic shock 'by dinner time' then by a stronger shock 'by bed time' (Vogt 1979). According to several historical sources, strong aftershocks occurred monthly for more than a year. Contemporaneous damage descriptions following the earthquake were thoroughly reviewed by Montandon (1943), Mayer-Rosa & Cadiot (1979), Vogt (1979), Lambert (1997) and Fäh *et al.* (2003). The city itself endured very severe damage with almost all of its churches and towers destroyed as well as part of the city moat and not more than 100 houses resisted collapsing (Vogt 1979). Earthquake victims may have reached 2000 lives from the 6000 inhabitants. This estimate can be, however, exaggerated as the region endured a 'black decade' that included a millennial flood in 1343, the Black Plague in 1348–49 and the Basel earthquake in 1356. Historical sources report that 40 castles were destroyed or heavily damaged within a 20-km radius of the city and damage to bell towers was recorded as far as 110 km in Strasbourg and Dijon. Mayer-Rosa & Cadiot (1979) assigned an intensity of IX-X on the MSK scale and an estimated magnitude of 6.0–6.5. Taking into account all historical observations and in the frame of the recently re-evaluated historical catalogue of the Swiss Seismological Service (Fäh *et al.* 2003), we propose a new

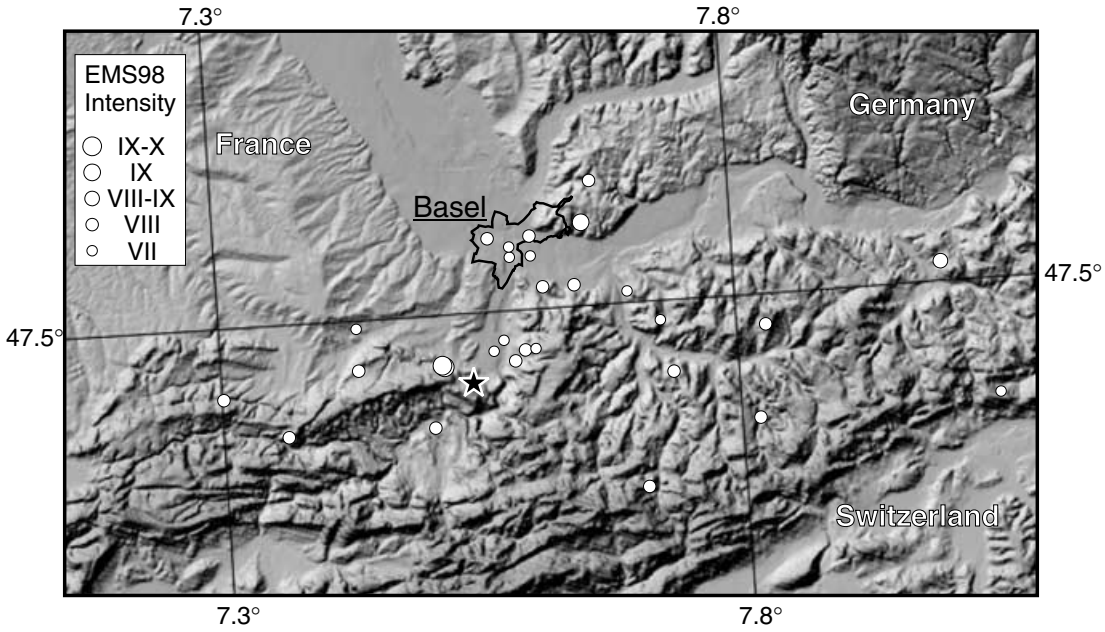

Figure 2. Intensity map for the 1356 October 18 Basel earthquake with data from the Swiss Seismological Service re-evaluated historical seismicity catalogue (Fäh *et al.* 2003). White dots indicate damage distribution. The inferred epicentre (black star) is located at the southern end of the Birs valley, 8 km south of Basel.

intensity map (Fig. 2). Soon after the earthquake, Pope Innocent VI sent a delegate who accurately described damage to the city and its surroundings. He reported that '. . . the earth opened in several places and white boiling sulphurous water flowed out abundantly.' (Vogt 1979) indicating the possible occurrence of surface ruptures and/or liquefaction features. In addition to the 1356 event, the region has seen nine other events with estimated magnitudes larger than 5 during the last millennium (Fäh *et al.* 2003).

3 NEOTECTONIC AND SEISMOTECTONIC FRAMEWORK

The Upper Rhine graben is part of a continental rift affecting intraplate Europe during late Cenozoic time. According to seismic profiles and borehole data, it is filled with more than 3300 m of Tertiary and Quaternary sediments (Doebel & Olbrecht 1974) . The southern region of the Upper Rhine graben (Fig. 3) is limited to the east by the tabular Jura and to the south by the folded Jura. Early extensional movements took place during the late Eocene and the late Oligocene and, according to Laubscher (2001), the tabular Jura is related to the extensional movements of the graben. In fact, along with a well-developed bounding fault system, the large-scale N–S trending Rhine valley flexure formed and a normal fault system propagated eastwards over more than 20 km, as far as Zeiningen (Fig. 3). This region is interpreted as the faulted upper Muschelkalk limestone forming individualized blocks tilted to the east and that slipped westwards on an underlying evaporite layer. The faulting episode presumably stopped during the late Oligocene and became a major west-dipping normal fault zone affecting the eastern rim of the tabular Jura. No mention exists in the literature on the Neogene and Quaternary tectonic episodes of this region.

To the south, the folded Jura forms an E–W arcuate folding system and constitutes the foreland tectonic structures of the western Alps. It is generally associated with the Alpine compression and is often interpreted as the most active structure in the region. Recent stress measurements (Becker 2000) and geodetic measurements (conventional and GPS, Nocquet *et al.* 2001) document Quaternary as well as present-day N–S to NW–SE compression and E–W to NE–SW extension of the main active deformation between the Jura and the Rhine graben. From geomorphic data and seismic profiles Nivière & Winter (2000) provide evidence for Quaternary faulting from a shallow (2–3 km depth) compressional décollement extending north in the Sundgau, but as a result of its geometry and depth it is not considered a seismogenic structure. Authors infer that the northern rim of the folded Jura exhibits several chevrons that would accommodate for most of the Quaternary compression. Although no evidence is shown for late Pleistocene and Holocene faulting, an inferred WSW–ENE basement fault has been considered as the most probable source for the Basel earthquake (Meyer *et al.* 1994).

The present-day stress tensor as inverted from focal mechanisms by Plenefisch & Bonjer (1997) corresponds to a predominantly strike-slip regime with σ_1 striking N162 and σ_3 striking N69, both of them being horizontal to subhorizontal. However, the presence of two secondary minima suggests that σ_1 may be oriented vertically or at 45°. Furthermore, as magnitudes between 2 and 4 only were available, implications in terms of crustal deformation should be cautious and extension may be considered likewise.

4 FAULT SCARP GEOMORPHOLOGY

The Rhine graben exhibits a N10–N20 direction and is in the south bordered by the Vosges massif to the west and the Black Forest massif to the east. South of the city of Basel, the recently identified BR fault forms the bounding structure of the Birs valley to the east with the Bruderholz heights to the west and exhibits evidence for a late Pleistocene and Holocene tectonic activity (Meghraoui *et al.* 2001). Its orientation (N15) is consistent with the general direction of the graben (Fig. 1). West of the Birs valley, the Birsig river flows eastwards to the western flank of the Bruderholz block then is sharply

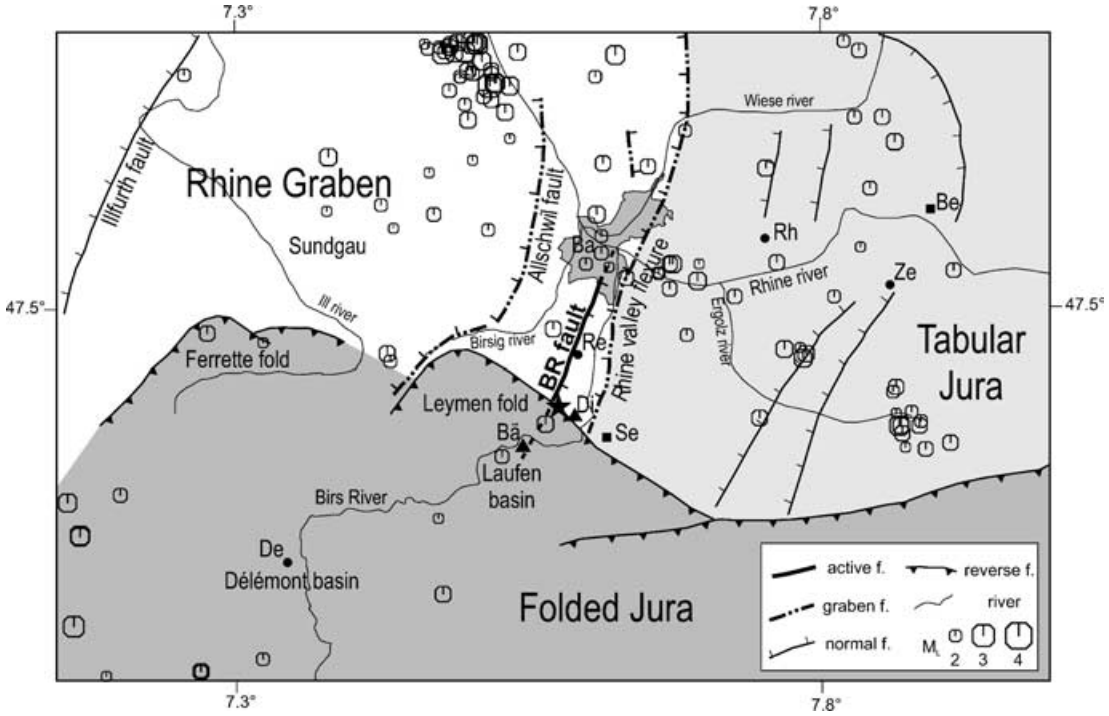

Figure 3. Seismotectonic framework of the southern upper Rhine graben. BR: Basel–Reinach fault, Ba: Basel, De: Délémont, Re: Reinach, Rh: Rheinfelden, Ze: Zeiningen. Seismicity recorded over 1975–2000, $2 < M_L < 4$. Black star refers to the location of the 1356 epicentre as estimated by the Swiss Seismological Service (Fäh *et al.* 2003). Triangles refer to caves investigated by Lemeille *et al.* (1999), Di: Dieboldslöchli, Bä: Bättlerloch. Squares refer to lakes investigated by Becker *et al.* (2002), Se: Seewen, Be: Bergsee.

diverted to the north (Fig. 3). As a response to a marked topographic asymmetry, drainage patterns on the eastern flank of the Bruderholz block display long meandering streams with short straight streams on its western flank (Figs 4 and 5a). The northern section of the BR scarp shows a series of streams that have incised ∼25 m through Quaternary river terraces and have steep (>40°) slopes. This geomorphology suggests intense erosion processes, which may be related to recent uplift or subsidence movements along the scarp. At the same location, two former meanders of the Birs river (see yellow dashed arcuate lines on Fig. 4) are now perched at 30–40 m relative to the present-day flood valley. More to the south and west of Reinach, the Erlenhof valley could be a similar younger feature. All along the BR fault scarp, Quaternary alluvial terraces attributed to the Rhine and Birs rivers crop out as elongated strips at various elevations above the Birs level. An examination of Quaternary terraces on both sides of the Birs valley shows that the top surface of the Q3s terrace (high terrace on Fig. 4), which is attributed to the ∼240 000 yr Riss age (Bitterli-Brunner & Fischer 1988) crops out at a higher elevation on the western flank of the valley (Figs 4 and 5b). Outcrops of Q3s follow a gentle gradient of ∼0.5° to the NNE on both edges of the Birs valley. However, their altitude is consistently higher by ∼35 m on the western side than on the eastern side. This indicates a minimum uplift of 30–40 m along the Bruderholz scarp with respect to the rim of the tabular Jura after the deposition episode of unit Q3s. Assuming a maximum age of 240 000 yr for Q3s and not taking erosion into account, we obtain 0.12–0.16 mm yr^{-1} as a minimum long-term vertical displacement rate.

At depth, the BR fault intersects an east-dipping normal fault as displayed on commercial seismic profiles (Bitterli-Brunner & Fischer 1988). Fig. 6(b) shows the profile BL24 in the vicinity of Basel, for which we had access to full-length original hard copies. At a depth of approximately 600 m, a sharp horizontal reflector (attributed by the authors to the base of the Tertiary) shows 100 m of vertical displacement along a system of high-angle normal faults. The upward prolongation of the main branch intersects the surface at the eastern edge of the BR fault scarp.

5 GEOPHYSICAL INVESTIGATIONS

To investigate the near-surface geometry of the fault and show its continuity from depth to surface, we selected three sites (Fig. 4) and conducted geophysical surveys with various resolutions and penetration depths. They proved to be efficient in locating faults and related features within the shallow subsurface at places where the geomorphologic signature is weak and/or concealed (Camelbeeck & Meghraoui 1998; Meghraoui *et al.* 2001).

Hence, a 600-m-long high-resolution seismic line was acquired across the scarp at site 2 (Fig. 7). Using a weight dropper and dynamite, we achieved a penetration larger than 200 m with an estimated vertical resolution of 20 m. At the western end of the profile, which is the top of the scarp, a continuous high-energy reflector dips gently to the west (∼15°). According to borehole data (Bitterli-Brunner & Fischer 1988), this reflector marks the base of Quaternary gravel deposits (Jüngerer Deckenschotter). It is vertically displaced by 80 ± 20 m along a system of normal faults, which form a graben. At the toe of the scarp, the Quaternary units are faulted and show ∼15 m vertical displacement. This is consistent with field observations and borehole data (Bitterli-Brunner & Fischer 1988). Hence, the base of the Quaternary units (Jüngerer Deckenschotter) shows a minimum 100 ± 20 m of vertical displacement from its topmost position on the scarp to the bottom of the valley. The base of the Quaternary north of the Bruderholz scarp exhibits a negative magnetic field

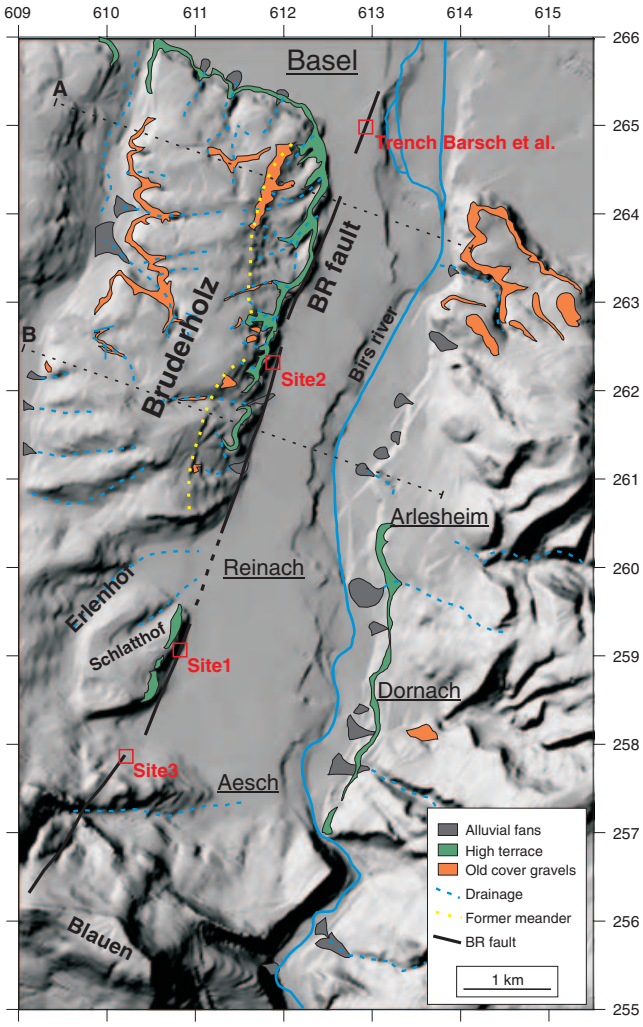

Figure 4. Geomorphology of the Basel–Reinach (BR) fault scarp. Shaded relief of the Birs valley from digital elevation data (DHM25 data set by Landestopographie, DV1441) shows the location of the BR fault (thick black line). Quaternary alluvial terraces (old cover gravels as orange patches and high terrace as green patches) and abandoned meanders (yellow dashed arcuate lines) of the Birs river are uplifted with respect to the present-day flood valley. Short straight lines on the eastern side of the valley are the result of kriging artefacts and old river channels. Black dashed lines labelled A and B refer to the extracted topographic profiles shown in Fig. 5. Coordinates are in kilometres in the Swiss CH1903 reference system.

that indicates an age older than the Bruhnes–Matuyama magnetic reversal (730 000 yr, Zollinger 1991). This yields 0.11–0.16 mm yr^{-1} for the long-term maximum vertical displacement rate in agreement with the 0.14 mm yr^{-1} obtained from the uplifted Q3s terrace. Furthermore, this suggests that seismic activity along the BR fault is probably not older than the Riss ice age (∼250 000 yr).

To improve details in the subsurface, we also conducted multi-electrode resistivity tomographic surveys (Suzuki *et al.* 2000). Two main electric units were repeatedly imaged (Fig. 8): a resistant material (100–400 Ω.m) probably composed with carbonates and always located near the surface and a conductive unit (5–40 Ω.m), probably clayey and silty, systematically located below or against the resistive unit. As measured resistivity values were very low, especially close to the surface, we could not use the ground-penetrating radar (measured resistivity should be larger than 50 Ω.m for 100-MHz antennae, see Meschede *et al.* 1997). We retained three alternative criteria for fault identification: (i) a distinctly vertically displaced resistivity unit, (ii) a sharp subvertical contrast separating two different units (lithological contact) or (iii) a subvertical intrusion of low-resistivity material associated with water circulation and possible secondary clay minerals deposition along a fault plane (Fujimoto *et al.* 2000).

At site 1, profile GE7 (Fig. 8) displays faulted blocks that are vertically displaced by approximately 9 m on two different fault strands to form a step-like morphology. They are overlain with a continuous conductive unit, probably composed with redeposited clayey loess washed off from the uppermost terrace surfaces.

At site 2, profile GE3 shows a graben-like structure that buries conductive material by more than 11 m (penetration depth of the method) in the graben. Profile GE4 exhibits a patch of resistive material similar to what is observed on the other profiles. This could be a block of the high terrace buried by the fault. Furthermore, it is overlain with an ∼2-m-thick conductive unit, which we interpret as water-saturated loess deposits. Considering that the loess/high-terrace contact could be located at a depth of 4 ± 1 m and that it can be correlated with the high terrace observed at 5 ± 1 m above the topography on the footwall block, this would suggest 9 ± 2 m of vertical displacement on that fault strand since the deposition of the loess layer, probably older than 26 900 yr (see TL dating Section 6.2.2) and probably younger than the Wurm last glacial maximum estimated at 70 000 yr (Bitterli-Brunner & Fischer 1988). This yields a minimum vertical displacement rate of 0.1–0.15 mm yr^{-1} on that fault branch for the Holocene and late Pleistocene, in fairly good agreement with results from geomorphologic and seismic investigations. According to these promising results, trenches were excavated at sites 1 and 2 on the exact location of profiles GE3, GE4 and GE7.

6 PALAEOSEISMIC TRENCH ANALYSIS

Geomorphologic as well as geophysical results led us to consider several sites favourable for trenching operations. As a result of the high density of buildings and thick vegetation cover along the scarp, available sites were much fewer than previously thought. However, original geomorphology with uplifted terraces and sources of recent sedimentation along the fault scarp were the main criteria for palaeoseismic site selection (Figs 4 and 8).

On the southern section of the fault (site 1) exploratory short trenches were dug in year 1999 to identify recent deformation structures and faulted young deposits and characterize a proper candidate for the source of recent earthquakes.

Site 2 is located 3.5 km to the NNE and was subsequently selected for a detailed palaeoseismic study. Although hidden by a small forest, a well-individualized fault scarp offers a clear topographic signature as well as favourable geomorphic features with colluvial and alluvial deposits associated to a recent drainage system.

Age determinations were performed using AMS radiocarbon and TL methods. More than 50 samples of organic material including charcoal fragments, bulk soil and a dog tooth as well as 15 sediment samples for TL analysis were collected in trenches (see Tables 1–3 in data repository). Charcoal fragments are of good size and shape because they have probably been produced locally since the Bronze age (Marti, private communication, 2002). Radiocarbon samples were prepared following the standard procedure described by Schleicher *et al.* (1998). Calibrated dates (BC/AD) were calculated using the OXCAL software (Bronk Ramsey 1995) along with the

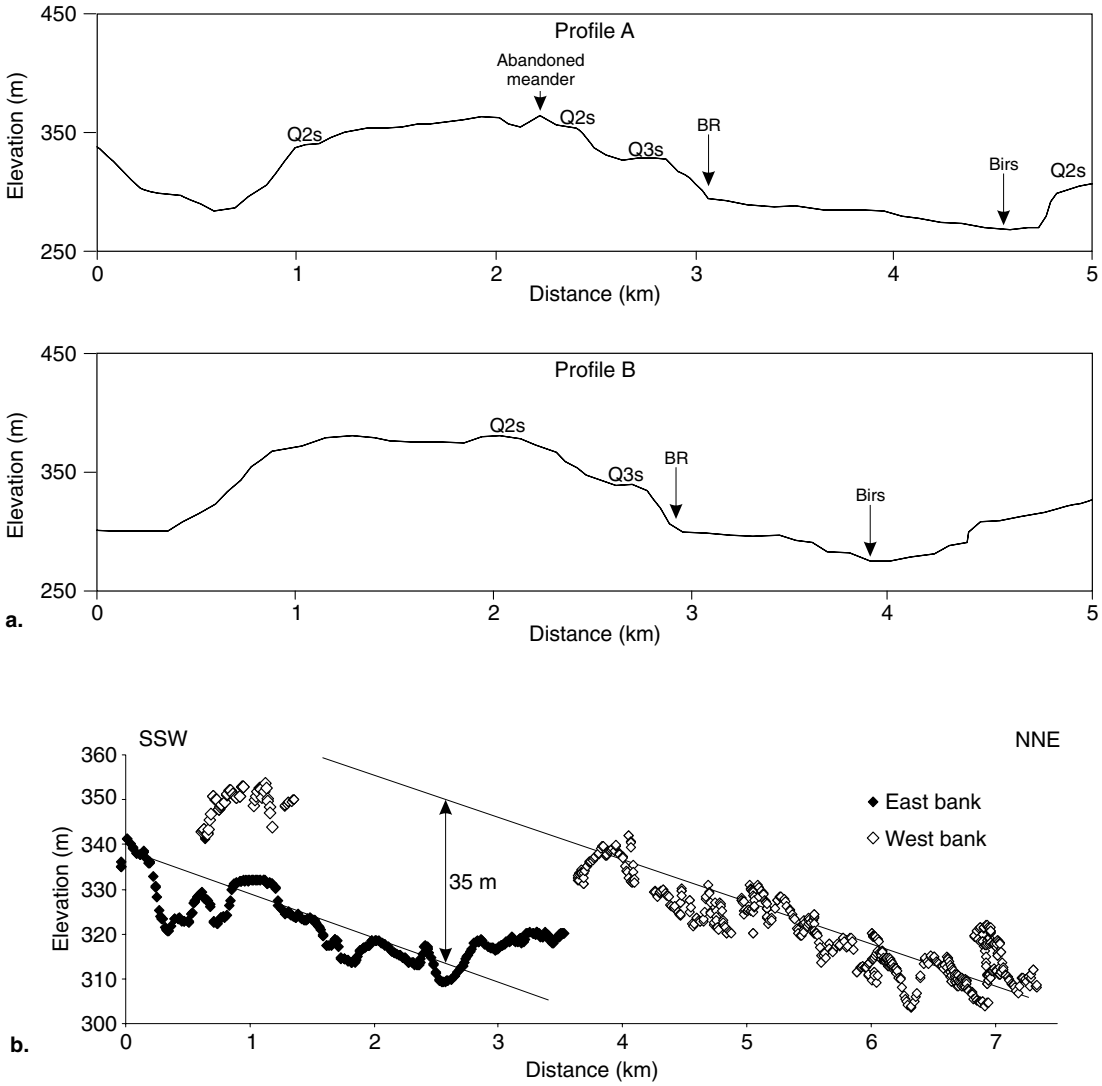

Figure 5. (a) Across-strike topographic profiles extracted from the DHM25 elevation data set show the asymmetry of the Bruderholz scarp and the location of the Basel–Reinach (BR) fault (BR) and the Birs river. Topographic flats mark the location of Quaternary terraces Q2s and Q3s. Note the westward dip of Q2s and the difference in elevation between both sides of the valley for Q2s and the apparent absence of Q3s on the eastern side. (b) Distribution of the high terrace (unit Q3s) along the Birs river. White dots from the Bruderholz scarp (uplifted block) and black dots from the Rhine valley flexure (downthrown block) show a consistent vertical displacement of 30–40 m.

INTCAL98 calibration curve (Stuiver *et al.* 1998) and are given for a 2σ (95.4 per cent) confidence interval.

6.1 Site 1

Site 1 corresponds to the southern part of the fault, which is less urbanized and more accessible for field investigations (Fig. 9a, attached plate). Well-preserved and uplifted alluvial terraces outline the existence of recent tectonic movements along the fault scarp (unit c1, Fig. 9b).

Trenching operations at this site were difficult to lead mainly because of a dense network of gas and water pipes and because of a dense forest cover. Hence, we could only dig two parallel trenches (upper and lower parts of composite trench B, Fig. 9b) of 1 m width, 2 m depth and 6–10 m length across the toe of the scarp.

The bottom of trench A shows gently west-dipping (5–10 °) hardened sandy layers with interbedded clays the facies of which corresponds to the Oligocene substratum (unit g). Colluvial wedges (unit e) made of sandy clay with fine and coarse gravels with at the base an erosional surface (units f1–f2) made of fine gravels in a sandy clay matrix (whitish layers) overlay unit g. Units e, f and g show minor normal faulting with vertical displacements ranging between 0.03 and 0.62 m. Unit c1 is ∼1-m-thick, massive, silty clay with fine gravels overlaying the substratum g. With a flat top surface wedging out against the scarp, this unit may result from an old river-terrace meander. The height of the flat top surface is estimated at 3.5 m with respect to the valley flood field. In trench B the substratum is made of organic-rich clay and hardened sandy clay layers (units d1 and d2). Unit d3 is very similar to colluvial wedges e and covers d1 and d2 unconformably. Units c2 and c3 are present in both trenches and correspond to organic-rich colluvial deposits overlain by a brown soil with scattered gravels (units a1 and a2). In the lower part of the trench, units d1, d2 and d3 are faulted and units c2, c3, a2 and ps are warped. This active deformation with a prominent scarp showing approximately 0.6 m of vertical movement at the surface

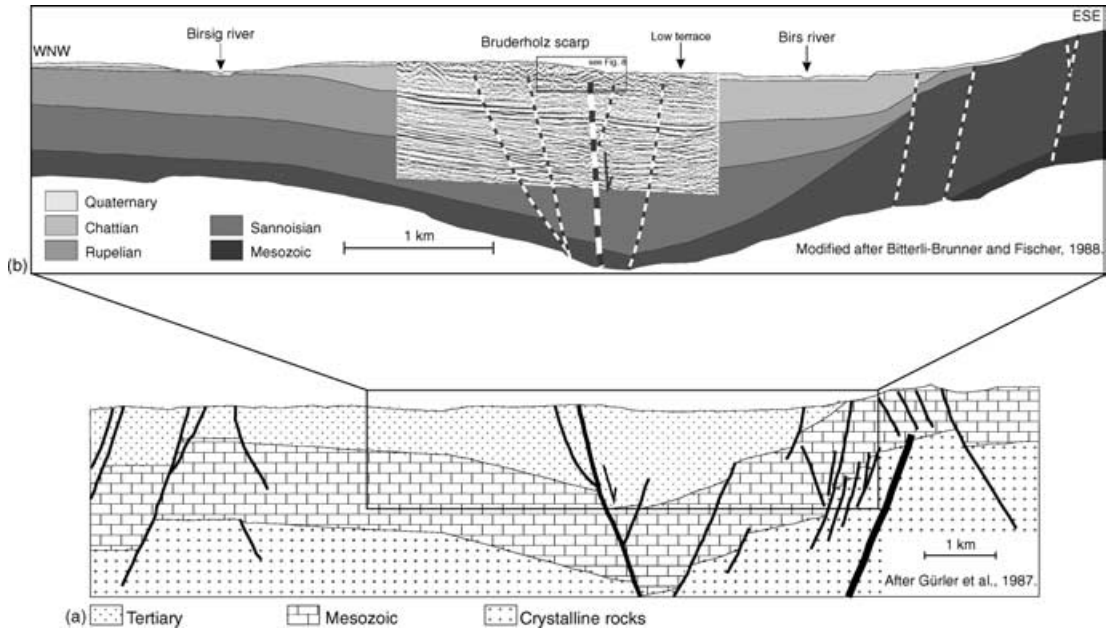

Figure 6. (a) General tectonic interpretation of the southeastern Upper Rhine graben by Gürler *et al.* (1987). (b) Public excerpt of commercial seismic line BL24 from 1978 within a general geological interpretation by Bitterli-Brunner & Fischer (1988). Note the near-vertical dip of the main fault at the eastern rim of the Bruderholz scarp. At a depth of ∼600 m, the base of the Chattian unit exhibits a clear seismic reflector. It is cut and vertically displaced by ∼100 m. Interpreted faults are stopped before reaching the surface as a result of improper resolution of seismics within the last 200 m. Vertical and horizontal scales are identical. Note that full-length profile and its exact location are not public data at the moment.

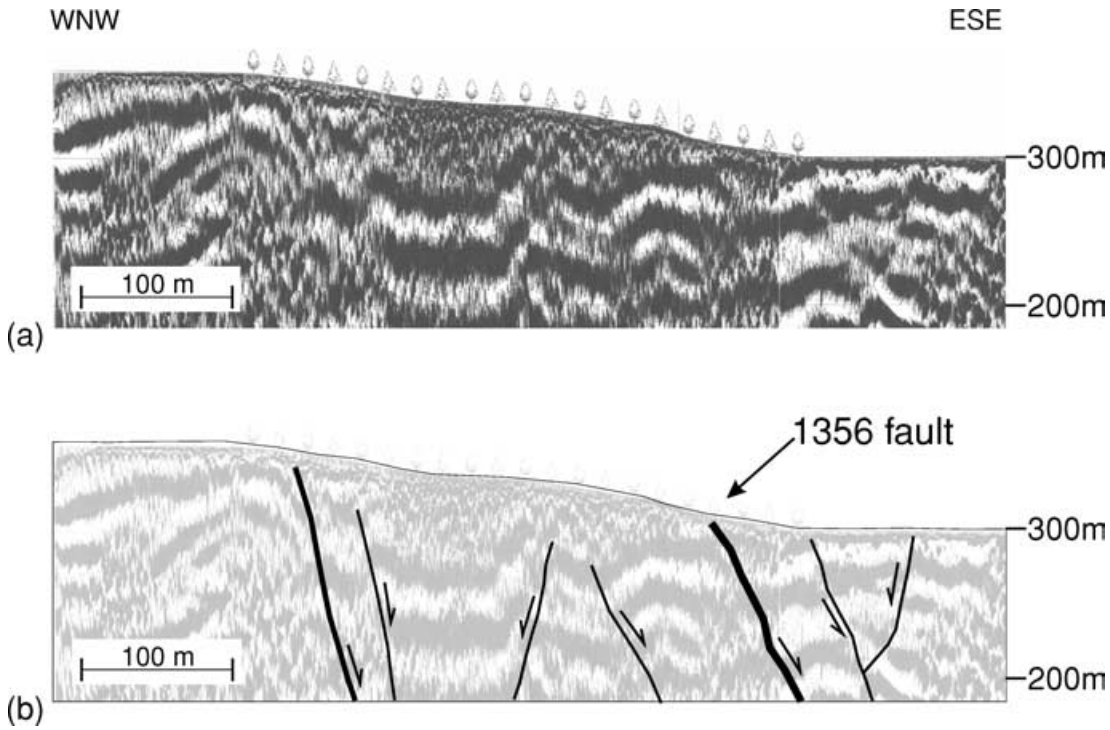

Figure 7. High-resolution seismic line surveyed across the Basel–Reinach (BR) fault at site 2, on the eastern flank of the Bruderholz block and the corresponding interpreted faults. This line follows a portion of the exact path of line BL24 (see Fig. 6) and resolves the uppermost 100 m of the fault system beneath the Bruderholz scarp. Again, note that faults are near-vertical.

topography testifies for the occurrence of a young faulting event. Similarly, unit a3 shows 0.6 m of vertical offset that is likely to be younger than c3 dated at 2470–2200 BC and may correspond to the AD 1356 Basel earthquake. The penultimate event that corresponds to faulted d1 and d2 can be bracketed between d2 (3270–2900 BC) and c2 (2560–2280 BC). An older event is suggested by the faulting of units f and e in trench C but no dating is available to determine the age.

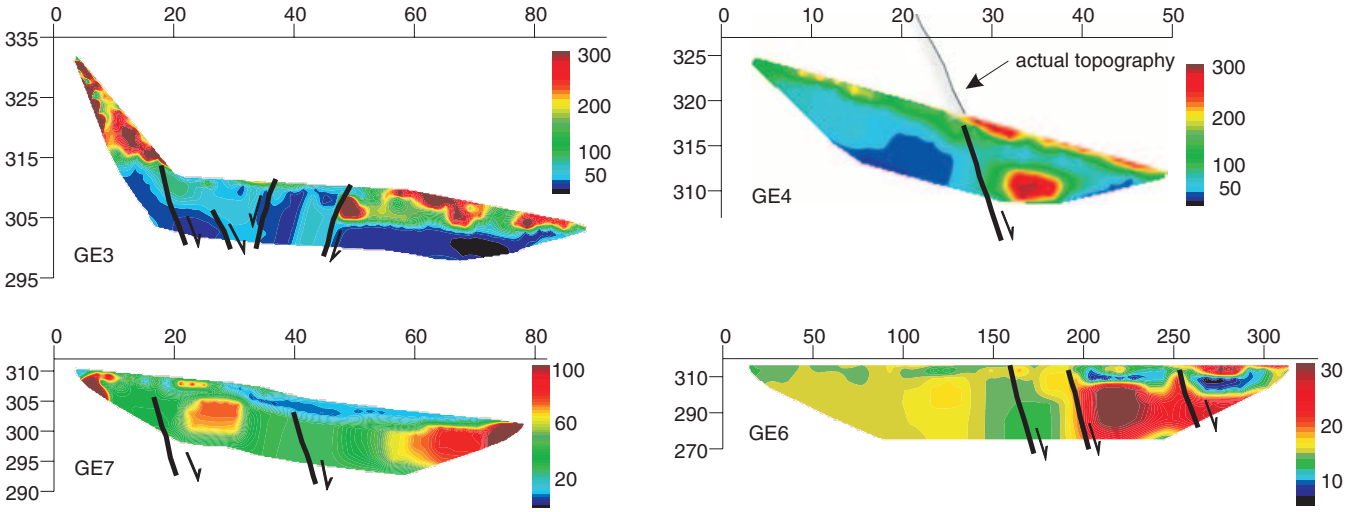

Figure 8. Electrical tomography data collected from west to east across the Basel–Reinach (BR) fault from north (top profile GE4) to south (bottom profile GE6). Modelled resistivity sections (left) are displayed with individually optimized colour scales. X coordinate is distance in metres from origin, y coordinate is elevation in metres above sea level. Resistivity is given in Ω.m. Black lines indicate inferred faults, which separate faulted and vertically displaced blocks.

6.2 Site 2

Site 2 is located on the northern section of the BR fault. This area is heavily urbanized and only a few locations are free of buildings. Six trenches were excavated for a total length of more than 230 m and a maximum depth of 4 m (Figs 9c–g). Oligocene deposits visible in the trench bottom, are composed with poorly cemented greyish sand with micas, clay lenses and seldom hard sandstone cobbles. These fluviolacustrine deposits are attributed to Chattian age as described in the Rhine graben (Alsatian molasse, unit O3, in Bitterli-Brunner & Fischer 1988). It is covered by the alluvial deposits of the high terrace (Q3s, Hochterrasse Schotter, upper Pleistocene) visible in trenches 4, 5 and 6. This unit is a polygenic conglomerate made of crystalline as well as limestone cobbles and pebbles from the Birs river with a sandy matrix and well-stratified sand lenses. It indicates a cold climatic environment and is associated with alluvial deposits of glacial origin. It can be continuously mapped northwards to the Rhine river where it is attributed to the Riss age (Bitterli-Brunner & Fischer 1988). The upper part of the section changes to a monogenic conglomerate of calcareous pebbles described as the Nagelfluh facies. Its matrix changes to a fine-grained unit of clay and silt probably secondarily deposited by the washing off of the upper loess cover. In trenches 1, 2 and 3, unit Q3s does not appear and Oligocene deposits are directly covered with late Pleistocene and Holocene deposits. These deposits are made of fine sands (probably resedimented loess deposits), gravels and fine gravels with a reddish brown and organic-rich clayey matrix. This may indicate a warmer climate with frequent rainfalls. In trenches 1 and 2, the top of the Oligocene exhibits a very corrugated erosional surface covered with conglomerates of calcareous pebbles with a sandy and clayey matrix. In trench 3, the Oligocene is overlain by (i) fan deposits at the foot of the steepest slope, (ii) interfingered gravels and silty clays on the lower half of the scarp and (iii) loess and massive dark brown soil at the toe of the scarp. In most places along the scarp, young deposits (Holocene) crop out as either alluvial deposits from the Birs river, fan deposits or colluvial deposits. Finally, as trenches 1 and 2 are very similar we document here only trench 1.

6.2.1 *Trenches 1 and 4*

Trench 1 (see Fig. 9f) is 88 m long and was dug at the same location as electric profiles GE2 and GE3. This trench did not show the main active normal fault but it displayed several minor antithetic faults. Indeed, we stopped the excavation upslope at the base of the scarp because of a tree. An additional trench was then opened 10 m aside, across the slope (see description of trench 4) below. The uppermost part of the trench, located on the flat surface, is composed with thick silty clays (unit c Fig. 9f) where four dated charcoal samples indicate a late Holocene age (see samples Grab1, Grab2, Grab3 and Grab4 in Table 2). Unit c does not show any visible layering and is probably resedimented reworked loess sediments. The antithetic faults present some characteristics of syn-sedimentary ruptures but the absence of clear stratified layers made difficult any assessment of successive faulting episodes. The eastern half of trench 1 presented a thick unit of conglomerates with centimetre to decimetre size that probably belongs to the lower terrace (Table 3). As shown in Fig. 9(f), the sandy clay substratum (attributed to Oligocene) is truncated (erosion surface) and overlain by the conglomerates. We interpret these outcrops of a deformed old alluvial terrace over the substratum, which forms an individual tectonic block (horst) near the main active fault and a small graben-like structure filled by unit c. In short, although trench 1 did not show a chronology of palaeoseismic events, it provides evidence for recent active deformation.

Moreover, it is of interest to mention the probable existence of the remains of a Roman road (Marti, private communication, 2002) which consists of a 10-cm-thick sandy gravels layer at the toe of the scarp (within unit a, Fig. 9f). The road seems to be strongly warped with ∼1 m of vertical separation suggesting the presence of a fault at depth and a recent coseismic movement. On the other hand, resistivity profile GE2 confirms that the warped geometry could be associated with a deeper fault. On the other side of the road, a construction pit (see eastern section of Fig. 9f) displays more than 4 m of alluvial loam and gravels (unit e, Fig. 9f). According to the resistivity and borehole data from the geological map, the contact between unit e and the Oligocene sands should be at 5 to 7 m depth.

Table 1. Results for radiocarbon AMS datation of 45 samples from the Basel–Reinach (BR) fault. Age determinations were performed by the Leibniz Labor of the Christian Albrecht University, Kiel, Germany (samples KIA) and the University of Zurich/ETH-Zurich, Switzerland (samples ETH). Conventional ages are 2σ-calibrated using OXCAL software (Bronk Ramsey 1995).

Location	Depth (m)	Sample name	Lab code	Material	Fraction	Amount of Carbon (mg)	Corrected pMC	d13C (per cent)	Radiocarbon age (BC) (BC)	Uncertainty (yr)	Calibrated date (+ = AD) 2σ range (95.4 per cent confidence)	
Trench 1	2	Grab 1	KIA12216	Charcoal	Alkali	3.1	58.22	−26.91	4345	35	−3090	−2880
Trench 1	2	Grab 1	KIA12216	Charcoal	Humic	2.2	59.39	−25.39	4185	30	−2890	−2630
Trench 1	2	Grab 2	KIA12217	Charcoal	Alkali	4.2	60.49	−27.90	4040	35	−2840	−2460
Trench 1	2	Grab 3	KIA12218	Charcoal	Alkali	3.9	69.96	−27.67	2870	30	−1190	−920
Trench 1	2	Grab 4	KIA12213	Charcoal	Alkali	4.3	65.61	−25.20	3385	45	−1870	−1520
Trench 3	1	F2.2N	KIA12214	Charcoal	Alkali	5.2	76.23	−25.77	2180	35	−380	−110
Trench 3	1	F2.2N	KIA12214	Charcoal	Humic	0.9	75.31	−26.79	2280	35	−410	−200
Trench 3	1	F2.3N	KIA12220	Charcoal	Alkali	1.1	75.05	−25.57	2305	30	−410	−230
Trench 3	1	F2.4N	KIA12215	Charcoal	Alkali	0.8	76.33	−26.97	2170	35	−370	−100
Trench 3	1	F2.5N	KIA12221	Charcoal	Alkali	5	30.04	−27.95	9660	45	−9240	−8800
Trench 3	1	F2.5N	KIA12221	Charcoal	Humic	3.6	30.78	−24.37	9465	50	−9150	−8600
Trench 3	1	F2.6N	KIA12222	Charcoal	Alkali	0.3	71.36	−30.66	2710	70	−1020	−760
Trench 3	1.5	F2.7N	KIA13416	Charcoal	Acid	0.5	35.49	−28.46	8320	85	−7550	−7080
Trench 3	1.7	F2.8N	KIA13417	Charcoal	Acid	1.2	74.97	−25.13	2315	30	−410	−230
Trench 3	1	F2.9N	KIA13418	Charcoal	Acid	0.6	31.66	−28.71	9240	80	−8690	−8270
Trench 3	1	F2.10N	KIA13419	Charcoal	AAA	0.8	75.31	−26.47	2280	35	−410	−200
Trench 3	1.5	T3.T01	ETH-25836	Dog tooth	AAA	1.6	78.3	n.a.	1915	50	−20	240
Trench 3	1.6	Tarc1	KIA12226	Charcoal	AAA	n.a.	77.28	−26.10	2020	40	−160	80
Trench 3	2.6	Tarc2	KIA12227	Charcoal	AAA	n.a.	59.43	−23.00	4130	40	−2880	−2570
Trench 4	0.7	CW1-1a	KIA12605	Bulk soil	Alkali	1.3	76.71	−25.07	2130	30	−360	−40
Trench 4	0.7	CW1-1a	KIA12605	Bulk soil	Humic	1.2	81.81	−24.27	1610	30	390	540
Trench 4	0.7	CW1-1b	KIA12606	Snail shell	Alkali	0.7	25.65	−7.08	10930	90	−11250	−10700
Trench 4	0.5	CW1-2	KIA12607	Bulk soil	Alkali	1.4	94.41	−27.34	460	25	1410	1475
Trench 4	0.4	CW1-3a	KIA13420	Bulk soil	Alkali	2.9	97.27	−25.35	225	30	1630	1950
Trench 4	0.4	CW1-3b	KIA13421	Charcoal	Alkali	4.7	98.55	−27.25	120	25	1670	1960
Trench 4	0.8	CW1-4a	KIA13422	Bulk soil	Alkali	0.8	70.79	−25.09	2775	35	−1000	−830
Trench 4	0.8	CW1-4a	KIA13422	Bulk soil	Humic	0.5	82.06	−28.05	1590	40	380	570
Trench 4	0.8	CW1-4b	KIA13423	Charcoal	Acid	0.5	94.88	−28.98	420	40	1410	1630
Trench 4	1.5	CW2-1	KIA12608	Bulk soil	Alkali	1	37.86	−27.45	7800	50	−6800	−6450
Trench 4	1.1	CW2-2	KIA12609	Bulk soil	Alkali	0.9	57.16	−25.43	4495	60	−3340	−3090
Trench 4	1.1	CW2-2	KIA12609	Bulk soil	Humic	1.2	70.78	−24.84	2775	35	−1000	−830
Trench 4	1.4	CW2-3	KIA13424	Bulk soil	Alkali	1.4	58.40	−26.95	4315	35	−20	−2880
Trench 4	1.4	CW2-3	KIA13424	Bulk soil	Humic	0.6	60.20	−26.50	4075	45	−2870	−2470
Trench 5	1.4	T5.C03	ETH-25832	Charcoal	Alkali	0.7	67.98	−23.90	3050	65	−1450	−1110
Trench 5	2.25	T5.C07	ETH-25833	Charcoal	Alkali	0.9	28.51	−21.20	10030	85	−10150	−9250
Trench 5	2.3	T5.C12	ETH-25834	Charcoal	Alkali	1.6	24.94	−17.50	11105	85	−11450	−10700
Trench 5	3	T5.C16	ETH-25835	Charcoal	Alkali	0.3	25.05	−23.40	11070	145	−11500	−10700
Trench 5	0.65	T5.S02	ETH-25837	Bulk soil	Alkali	1.6	99.19	−22.70	Modern	n.a.	n.a.	n.a.
Trench 5	0.7	T5.S03	ETH-25838	Bulk soil	Alkali	1.4	100.68	−26.10	Modern	n.a.	n.a.	n.a.
Trench 5	1.55	T5.S04	ETH-25839	Bulk soil	Alkali	1.6	39.78	−19.90	7355	70	−6390	−6060
Trench 5	0.5	T5.S05	KIA-19082	Bulk soil	Alkali	2.6	73.54	−26.39	2025	25	−100	60
Trench 5	0.5	T5.S05	KIA-19082	Bulk soil	Humic	1.2	88.80	−33.73	1265	25	670	860
Trench 5	0.7	T5.S06	KIA-19083	Bulk soil	Alkali	1.2	86.17	−22.34	1195	25	770	940
Trench A	n.a.	Tal4	Beta-135096	Charcoal	AAA	n.a.	81.63	−26.40	1580	40	400	600
Trench A	0.65	TB2˙N5	Beta-135094	Charcoal	AAA	n.a.	61.46	−25.60	3860	40	−2470	−2200
Trench A	1.65	TB2˙S4	Beta-135095	Plant	AAA	n.a.	57.53	−29.70	4390	40	−3270	−2900
Trench A	n.a.	TC˙nord1	Beta-135093	Charcoal	AAA	n.a.	46.33	−24.70	6130	50	−5260	−4850
Trench A	0.4	TC˙sud3	Beta-135092	Charcoal	AAA	n.a.	61.00	−24.90	3920	40	−2560	−2280

Combining resistivity with trench 1, we may correlate the flat bottom of the lower terrace (unit e in Fig. 9f) at location 35 m with the same lower terrace limit at location 105 m and infer a minimum 8 m of vertical displacement. According to the geological map (Bitterli-Brunner & Fischer 1988), the lowerace should have taken place after the last glacial maximum, i.e. ∼70 000 yr ago (Wurm age). This leads to a minimum 0.11 mm yr^{-1} vertical displacement rate for the late Pleistocene and Holocene along this branch of the normal fault.

Trench 4 was excavated across the steepest part of the scarp, at the western end of trench 1. It exhibits a clear normal fault rupture up to the surface with alluvial terrace deposits on the footwall block (Riss-age high terrace, unit j on Fig. 9d) juxtaposed to colluvial wedges with Holocene sandy silt and gravel in the hanging block. The fault

Table 2. Stratigraphic units related with the Birs Valley and the Basel–Reinach fault scarp. Climate from Haas *et al.* (1998) and Magny *et al.* (2001).

		Climate	Trench 1	Trench 3	Trench 4	Trench 5	Trench A	Trench Barsch	
Holocene				unit a	unit a	unit a	unit a		Event Z
			unit a	unit b		unit b	unit b		
			unit b	unit d1	unit c	unit c	unit c		Event Y
			unit c				unit d		
				unit c1					
				unit d2	unit d				Event X
					unit e	unit e			
				unit c2					
				unit d3	unit f	unit f			Event W
Pleistocene	Würm			unit c3	unit g	unit g			
					unit h	unit h			
				unit d4					Event V
				unit c4	unit i	unit i			
				unit d5					
				unit e					
			unit e	unit f				unit a	
	Riss			unit g	unit j	unit j		unit b	
Miocene								unit c	
								unit d	
Oligocene			unit f	unit h	unit k	unit k	unit g	unit e	

Table 3. Thermoluminescence (TL) datation results for nine sediment samples from the Basel–Reinach (BR) fault.

Location	Sample name	Age BP (yr)	Uncertainty (yr)	Date BC		Observation
				Minimum	Maximum	
Trench 3	BAS51	25 800	3100	26 900	20 700	
Trench 3	BAS52	14 720	1490	14 210	11 230	
Trench 3	BAS53	>119 000		117 000	n.a.	Older than TL range
Trench 3	BAS54	14 570	1570	14 140	11 000	
Trench 4	BAS31	9110	920	8030	6190	Correlates with ^{14}C sample CW2-1
Trench 4	BAS32	16 010	1790	15 800	12 220	
Trench 4	BAS33	12 870	1560	12 430	9310	
Trench 4	BAS34	18 790	2610	19 400	14 180	
Trench 6	BAS75	>119 000		117 000	n.a.	Older than TL range

shows an ∼10-cm-thick gouge zone with deformation bands of grey and white stiff clay and oriented pebbles and gravels. The uppermost Holocene units are made of three episodes of colluvial wedges (units a, c and d on Fig. 9d).

(i) Unit a is 30–40 cm thick and is made of well-stratified pebbles in a clayey matrix. It caps the fault, does not exhibit evidence for deformation and its base material has been dated AD 1410–1475 and AD 1630–1950 (see samples CW1-2 and CW1-3a in Table 2). Unit a is overlain with the present-day soil, which is ∼20 cm thick.

(ii) Unit c is 50–60 cm thick and shows at its base an erosional surface, which is marked by a group of mixed coarse and middle size gravels dated 360–40 BC and 1000–830 BC (see samples CW1-1a and CW1-4a in Table 1) and overlain by thinner levels of fine gravels in a sandy matrix.

(iii) The base of unit d also corresponds to an erosional surface where fine and coarse gravels lay on fine silty sand deposits dated 3020–2880 BC and 3340–3090 BC (see samples CW2-3 and CW2-2 in Table 1). This 0.8–1 m thick unit consists of well-stratified and nearly horizontal 5–10 cm thick sandy and gravel layers with graded bedding (fine elements to the top) bent and deformed near the fault.

The uppermost colluvial levels stratigraphy of trench 4 shows a rather consistent succession of seven ^{14}C ages.

The lower units e, f, g, h and i (Fig. 9d) are made of massive silt and clay with some aligned pebbles, which mark the stratigraphy. It consists of massive fine silt and brown clay with a very few gravels. We sampled for TL age determinations and yielded complicated results. The four samples BAS31 to 34 present a succession of ages 8030–6190 BC, 15 800–12 220 BC, 19 400–14 180 BC and 12 430–9310 BC, respectively, with BAS32 and 34 being on the same stratigraphic level. In this succession, as the lowermost level of unit e presents the youngest age (BAS31), these overlapping ages could be a result of reworked colluvial sediments, which are not suitable for TL dating method. Furthermore, unit e consists of very fine-grained sediments in a steep slope morphology that likely favours relatively fast sedimentation. Nevertheless, one may note that the sample BAS31, which is located at the lower part of unit e (see also Table 3) is in good agreement with the ^{14}C date 6800–6450 BC (see sample CW2-1 in Table 1). Taking into account this good correlation and the consistent ^{14}C ages of corresponding units c, e, f and g in trench 5 (see paragraph below), we think that the TL dating BAS32 to 34 in unit e may not reflect the true depositional age.

Unit f is strongly warped and faulted and shows 20 to 30 cm of vertical displacement across two fault splays, one of which presents a reverse geometry (Fig. 9d). These two minor fault ruptures indicate the occurrence of a faulting event that postdates unit f and probably

took place during the deposition of unit e. This observation may indicate the occurrence of a seismic event between 8030 BC and 6450 BC.

6.2.2 Trench 3

Trench 3 is 94 m long and was excavated in the footwall inside an incision and across the alluvial fan deposits down to the toe of the scarp (Fig. 9g). Here, the trench location depended on the existence of a path in between many trees and, although one may expect a strong erosional activity, it exhibited three major normal faults F1, F2 and F3 as well as numerous minor faults. Fault F1 is located at the base of the steepest slope and F2 is 35 m down the slope. F1 and F2 dip steeply to the east (∼65°) and show 10–20 cm thick altered gouge zones and deformation bands that include many oriented gravels and pebbles. On the hanging block of F1 and from the bottom of the trench, one may recognize three sequences of colluvial wedges made of coarse gravels with a sandy matrix (unit e1, e2 and e3) overlain by fine sands (unit e). The latter unit was dated at three places using TL, which provided ages ranging between more than 117 000 BC to 14 210–11 230 BC (see Fig. 9g and samples BAS52, BAS53 and BAS54 in Table 3). If these units can result from the erosion of fault scarps, each sequence may result from a scarp-degraded process and be correlated with a palaeoseismic event. Hence, the oldest observable event on that fault could have occurred before 117 000 BC with a vertical displacement of at least 0.5 m. Another palaeoseismic event may have taken place before 26 900–20 700 BC and be responsible for a minimum ∼0.5 m vertical slip as inferred from the thickness of colluvial units (Fig. 9g). A more recent palaeoevent took place before 14 210–11 230 BC and produced a larger displacement of ∼1 m. As inside any incisions, the uppermost overlaying deposits (alluvial fan deposits a1 and a2) truncate and cap the fault and erase the geological record (and most probably the most recent displacement). However, down the slope the four generations of fan units a1, a2, a3 and a4, reaching a total thickness of more than 3 m, were deposited after the erosional unit b (possibly artificial), i.e. after 410–40 BC (see samples F2.2N, F2.3N, F2.4N, F2.6N, F2.8N and F2.10N in Table 2). Moreover, ^{14}C dating of sample T3.T01 (lowermost deposits of unit a2, Table 4) indicates that units a1 and a2 are younger than 20 BC–AD 240. Recent movements on F1, which is truncated by a1 and affect a3, can be at the origin of the fast accumulation of the thick alluvial fan deposits and the most recent movement may have occurred after a2, i.e. after AD 240.

The second normal fault F2 exhibits a similar geometry with a minimum thickness of 5 m of accumulated recent deposits on the hangingwall (see Fig. 9g). Against the fault, unit d5 displays densely packed gravels with a cemented block of subvertically oriented pebbles and sandy layers. Close to the surface, unit c5, which is a 20-cm-thick silty loess layer dated 14 140–11 000 BC by TL (see sample BAS54 in Table 3), is strongly warped and faulted with ruptures showing a reverse geometry. TL dating of trench 3 concerned samples with a sedimentary environment characterized by both low-energy alluvial and colluvial deposits. This is attested by the small size and sandy silty units associated with channel structures and small to middle size conglomerates in colluvial wedge units. Hence, TL age determinations seem to be in good agreement with the stratigraphic succession and the ^{14}C datings.

Tectonic features of trench 3 near F2 can be interpreted as typical of hangingwall structures of a major normal fault (McCalpin 1996). Faulting events here are at least younger than 14 140 BC. A sequence of colluvial gravel wedges with units d1 to d4 alternating with thick (1–2 m) silty clay deposits of units c1 to c4 displays a consistent succession of TL and ^{14}C ages. In fact, ^{14}C dating of nine samples from units d4 to b spans the time between 8690 BC to 40 BC (see Fig. 9g, near fault F2). The hanging block shows a stratigraphy with a progressive dip of ∼0°, ∼8°, ∼19° and ∼30° illustrating an anticlockwise rotation increasing with distance from the fault. Four identified gravel wedges constitute reference levels, which are composed with rounded limestone gravels with no visible stratigraphy in a silty clay matrix similar to units c1 to c4. As these four units display a typical debris facies followed by a wash facies, they also contain elements only from the footwall and are incrementally deformed against the fault. We infer that they constitute a series of colluvial wedges associated to successive coseismic displacements on fault F2.

An alternative interpretation could be invoked explaining the progressive anticlockwise tilt of units d as gravity-related landslide process. This interpretation is not supported, however, neither by the antithetic normal faults located east of F2 (see F2', Fig. 9g) nor by the warped unit c5 with reverse geometry in the hanging block nor by the imbricated parallel main normal faults F1, F2 and F3 visible at the surface and at depth (see geophysical investigations). Moreover, deformation bands and warping of numerous white $CaCO_3$ levels in the footwall block near the gouge zone reflect the long-term deformation with a high level of friction that does not support the landslide interpretation. The microscopic study of grain size, related mineralogy and structure of the gouge zone reveals two stages of deformation with (i) a ductile deformation with folding and production of chlorite, and (ii) a brittle behavior with fractured minerals and development of illite in the gouge zone (Orellana 2002).

On the hangingwall, 3 m east of F2, unit b, which constitutes the base of unit a4, seems to be slightly warped and broken upon the flexured silt layer unit c5. It thickens to 1 m as it interfingers eastwards with the sequence of units d and c. The numerous ^{14}C datings of unit b (all younger than 410 BC) predate the youngest deformation event probably associated with a movement of a hidden fault at depth.

Between stations 65 and 75 m, thick gravel deposits (unit d5) display well-stratified levels with ∼20-cm-thick loess lenses, which are warped and displaced by minor antithetic normal faults with ∼10–20 cm vertical displacements. The easternmost loess lens is cut and displaced by a major antithetic normal fault that shows ∼1 m of vertical separation, truncated by the alluvial fan deposit unit a4. More to the east, several other antithetic faults marked by sandy lenses are sharply truncated by unit a4.

On the eastern side of the road, a team of archaeologists from the Canton of Basel opened several excavations in 1999, one of which is aligned with trench 3 (see lower section on Fig. 9g). The trench was enlarged for us to allow investigations on the fault zone. A small and well-expressed vertical fault with an ∼10-cm-wide gouge zone showing oriented pebbles and gravels and a clear cut of a pottery-rich Bronze Age unit were exposed (unit d in Fig. 9g). In this trench, the relationship between faulted d covered by units c and b (supposed Roman road) indicates the occurrence of the penultimate palaeoearthquake between 2880–2570 BC and 160 BC–AD 80 (see samples Tarc1 and Tarc2 in Table 1).

6.2.3 Trench 5

Trench 5 was excavated on a similar location as trench 4 and approximately 30 m to the south. It unveils very similar structures to trench 4 as well as complementary information on stratigraphy and successive faulting episodes (see Fig. 9c). A sharp rupture cuts

through alluvial terrace deposits (Riss-age high terrace, unit j) and slope deposits from the base of the trench up to a depth of 1 m below the surface. A 20–30 cm thick gouge zone displays deformation bands with two fault strands at depth with numerous oriented gravels and pebbles. As in all the other trenches opened at site 2, Oligocene sands (unit k) crop out at the base of the footwall and can be considered as the substratum (pre-Quaternary bedrock). At the contact between unit k and the main fault, a 40-cm-thick zone shows very high clay content, iron oxide colouration, a shear fabric and a significant increase of water content. Terrace deposits composed with conglomerates of crystalline origin, and boulders and pebbles in a sand-rich matrix (unit j) overlay the substratum. Two small secondary faults affect and displace sandy gravel units with ∼20 cm of vertical separation. Unit a, dated modern (see sample T5.S02 in Table 2), caps the fault and shows no sign of deformation. It overlays a 1–1.2 m thick unit made of massive clayey silts of modern age and contains some scattered gravels near the base (unit b). Unit b covers a wedge of 1-m-thick densely packed limestone gravels with a clayey matrix (unit c). That unit pinches out down slope and displays graded bedding upon an erosion surface. It is dated 1450–1110 BC (see sample T5.C03 in Table 2). Close to the main fault, unit c is ruptured and vertically displaced by two fault splays, which form a 30-cm-deep, small graben. Unit c lays unconformably over unit e, composed of massive brown clay with scattered limestone gravels. In accordance with age determinations from trench 4, the unit e topmost part is dated 6390–6060 BC (see samples T5.S04 and CW2-1 in Table 1), suggesting either an unlikely gap in sedimentation processes or a strong erosion of unit e before deposition of unit c. Unit e covers unit f, another colluvial wedge made of more or less stratified gravels in a dark clay matrix. Laying over an erosional surface, the base of unit f contains some large charcoal pieces (over 0.5 cm^3), one of which is dated 10 150–9250 BC. This is consistent with results from trench 4 where the base of unit e was dated 8030–6190 BC. Unit g is made of massive clayey silts, which contain some scattered gravels. A few imbricated pebbles suggest a source located up the slope and charcoal samples provided very close radiocarbon dates with 11 450–10 700 BC for the top and 11 500–10 700 BC for the base (see samples T5.C12 and T5.C16 in Table 1). Note that the content of carbon extracted from sample T5.C16 is very small (0.3 mg), which may not provide an accurate date. Underlying unit h is made of dark beige silts with gravels and dips ∼40° towards the valley. Its upper part is completely incorporated into the gouge zone and indicates a strong degree of deformation. Unit i is very similar to unit h but it contains fewer gravels. It is highly warped and deformed and almost completely reworked within the shear zone. Both units h and i do not contain enough organic material to ensure proper radiocarbon dating and their grain-size content is not suitable for TL analysis.

Trenching operations as well as subsurface geophysical surveys suggest that a young (Holocene) fault branch should be located exactly below the road. Approximately 50 m north of site 2, trench 6 (see Fig. 9a) was opened to check if a fault strand could be detected beside the road. Excavating operations were limited by man-made structures and stopped 4 m before reaching the road. The absence of a fault affecting young alluvial and colluvial units in trench 6 confirmed the geophysical results.

Commercial excavations opened in 1962 for construction purposes were located coincidentally on the northern continuation of the fault (Barsch *et al.* 1971). The authors provide a detailed geological description of trench walls and recognized clear fault ruptures affecting young sediments with oriented gravels and pebbles within a damage zone (Fig. 9e). The presence of a fault affecting late Quaternary units 2.5 km NNE of palaeoseismic site 2 and along the BR fault scarp indicates the likely northern continuation of the BR fault into the city of Basel.

7 SUMMARY

7.1 Palaeoseismic events inferred from trenching

The two palaeoseismic sites along the BR fault scarp have revealed evidence for Holocene and late Pleistocene normal surface faulting. Sedimentological conditions combined with the successive movements on the fault allowed the recording of past seismic events. Furthermore, the analysis of fault displacements and sedimentary units leads to the identification of coseismic events. We present in the following the successive palaeoseismic events beginning with the most recent.

(i) Event Z (AD 500–AD 1450): this event can be observed at site 2 on fault 1 (see unit a in Fig. 9d and unit a in Fig. 9c), on fault 2 as a flexure of units b and a4 and probably at site 1 (see warping of the present-day soil). It displays a minimum vertical displacement of 0.5 m. This yields a minimum moment magnitude of $M_w = 6.2$–6.5. We correlate the faulting event with the last known historical seismic event of AD 1356.

(ii) Event Y (2490 BC–2210 BC): this event can be observed at both sites on all major fault branches as very well expressed colluvial wedges (see unit c in Figs 9d and c and unit c3 in Fig. 9b). It was probably the strongest Holocene event on the BR fault. The minimum vertical displacement measured in trench 5 is 1 m, which yields a minimum moment magnitude of $M_w = 6.4$–6.7.

(iii) Event X (6200 BC–3200 BC): this event can be observed at site 2 on fault 1, inside trench 4 (see unit d in Fig. 9d). In trench 5, the very rough top surface of unit e suggests that intense erosion processes may have removed the corresponding event horizon. With a thickness of 0.8 m, unit c corresponds to a minimum $M_w = 6.4$–6.6 event.

(iv) Event W (8030 BC–7300 BC): this event is observed at site 2, on faults 1 and 2 and is associated with the well expressed colluvial wedge of unit d3 (Fig. 9g). The colluvial wedge displays a thickness of at least 0.7 m. This yields a minimum moment magnitude of $M_w = 6.3$–6.6 for event W.

(v) Event V (11 200 BC–9500 BC): this event is observed at site 2 on both fault 1 (see unit f in Figs 9c and d) and fault 2 (see unit d4, Fig. 9g). The associated colluvial wedge has a thickness of 0.8 m, which corresponds to a minimum $Mw = 6.4$–6.6 event.

Reconstruction of palaeoseismic events of Fig. 10 illustrates the successive faulting events in trenches 4 and 5. The Bayesian analysis of 17 radiocarbon dates and one TL age (Fig. 11) is performed on a stratigraphic sequence basis. Events are inserted with respect to their stratigraphic position. The output provides a consistent chronology of deposition and faulting where each sample is characterized by its agreement ratio within the model and an optimized time bracket for the occurrence of each event. This analysis is completed for each major fault branch and with a combination of observations from all trenches (Fig. 12). The synthesis of trench observations and correlation of faulting events indicates that events Z and Y are well constrained and their related surface ruptures were probably visible along most of the BR fault scarp. Events X, W and V are relatively less well constrained but the faulting analysis suggests that coseismic surface ruptures took place on both F1 and F2 fault branches. The palaeoseismic analysis shows that events Y and W are bracketed within 280 and 800 yr, respectively. These results allow

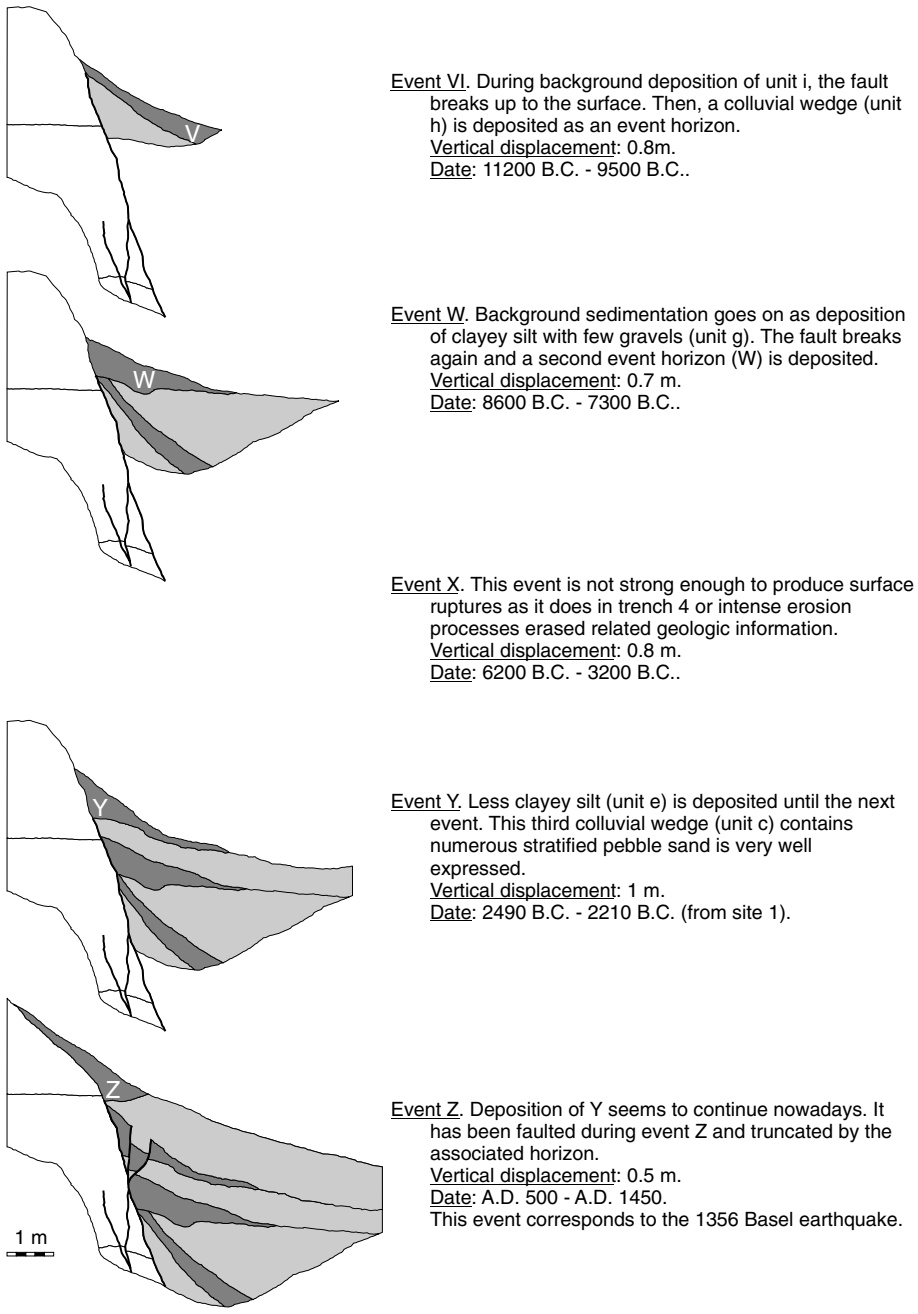

Figure 10. Reconstruction of faulting events identified in trench 5. Each event is characterized by its corresponding event horizon (colluvial wedge), the associated vertical displacement and the time range of occurrence for the event, as determined by the Bayesian statistical analysis (see Fig. 11). The last situation is the actual trench log (Fig. 9c).

us to extract an average recurrence interval of 2300–2600 yr for earthquakes similar to the 1356 event.

Moment magnitudes estimated following Wells & Coppersmith (1994) relations taking into account a fault length ranging from 11 to 15 km and a thickness of the seismogenic crust ranging from 12 to 20 km yield $Mw = 6.2$ to 6.7. However, for a normal fault scarp with displaced horizontal surfaces and related erosion processes (Wallace 1977), the thickness of a colluvial wedge may reach half of the coseismic scarp height, i.e. half of the vertical coseismic displacement (Fig. 12). The amount of vertical coseismic displacement could therefore be underestimated and a larger vertical slip would yield $M_w > 6.7$.

7.2 Events identified within other geological archives

Recent studies in the epicentral region of the 1356 Basel earthquake investigated various indirect evidence of past earthquakes using geological archives. Damage to speleothems were studied in two caves located on the Blauen anticline, south of the Birs valley (Fig. 3), and yielded the identification of an event dated AD 1165–1400 well correlated with the 1356 Basel earthquake (Lemeille *et al.* 1999). On the other hand, sedimentary records of lakes Seewen and Bergsee (Fig. 3) were drilled and dated and the seismites analysis permitted the detection of three events for the last 12 000 yr (Becker *et al.* 2002). Compared chronologies (Fig. 12) show a fairly good

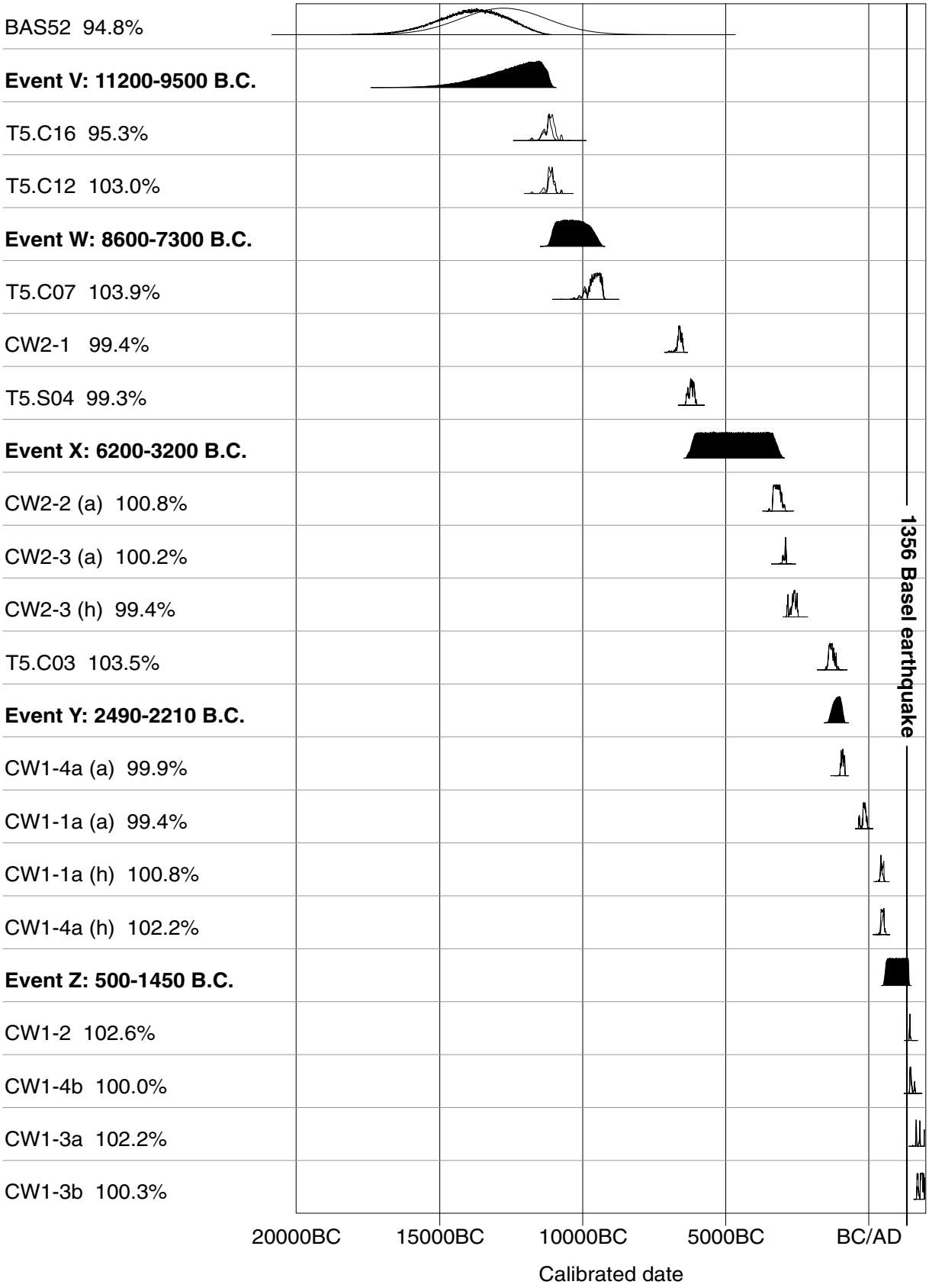

Figure 11. Bayesian statistical analysis of radiocarbon data for fault 1 at site 2. Radiocarbon ages are ordered in a sequence following stratigraphic relationships deduced from trench observations. Events were included on the same basis. Percentages indicate individual agreement of data within the sequence. Overall agreement is 100.2 per cent. Atmospheric data from Stuiver *et al.* (1998); OXCAL v3.8 see Bronk Ramsey (1995). The process was performed for each fault branch at each site and for the overall data set.

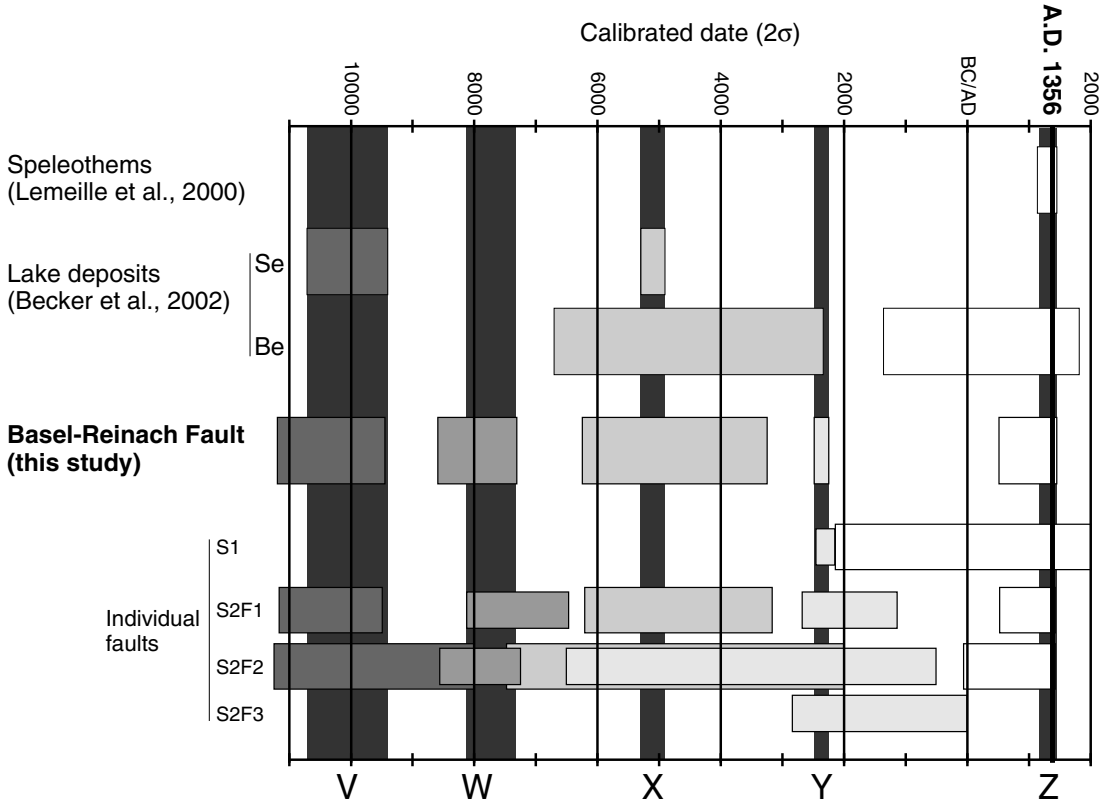

Figure 12. Holocene seismic history of the Basel–Reinach (BR) fault as deduced from trench investigations at sites 1 and 2 compared to events inferred from various independent geological archives in the epicentral area of the 1356 Basel earthquake. Light shades of grey refer to events identified for individual fault branches (S1: site 1; S2F1: site 2, fault 1; S2F2: site 2, fault 2; S2F3: site 2, fault 3) or individual archives (for lake deposits, Se is for Lake Seewen, Be is for Lake Bergsee. See Fig. 3 for location). Darkest grey indicates correlated events with time ranges minimized following individual datings. Note that events Z (1356 Basel earthquake) and Y clearly produced surface ruptures at both sites and along two of three branches at site 2. Older events X, W and V were only identified at site 2 but on two fault branches. Events Z and X are clearly correlated across independent geological archives (BR fault and lakes Seewen and Bergsee), thus potentially improving the datation of event X.

correlation between events X and V inferred from our palaeoseismic investigations and from speleothems study and seismites in Lake Seewen.

8 DISCUSSION

The identification of a seismic source for the 1356 Basel earthquake is achieved by means of a palaeoseismic analysis along an 8-km-long fault scarp. The successive vertical displacements on the BR fault and related colluvial wedges document the occurrence of five earthquakes in the last 13 200 yr and suggest a recurrence interval of ∼2500 yr for large to moderate earthquakes. The 54 dating results of radiocarbon and TL analysis provide the timing of the faulting episodes and yield an uplift rate of ∼0.27 mm yr^{-1} in the Holocene and late Pleistocene (Fig. 13a). This uplift rate averages at 0.1 mm yr^{-1} over the Pleistocene.

8.1 Faulting geometry and length extension

Trenches across the BR fault have revealed a complex surface faulting geometry. In trench 4, where the bedrock crops out over a depth of 2 m, the fault dips from 75°ESE as it cuts through a fluvial terrace (unit j) to 50°ESE in the bedrock (unit k). This suggests that significant opening may be expected as part of the coseismic displacement close to the surface. Besides, the 94-m-long trench 3 shows the existence of a double branching of the main fault to form *en échelon* blocks with probable simultaneous successive displacements. This is attested by the occurrence of well-expressed colluvial wedges on the hangingwall with progressive tilt of gravels and fine sand accumulation in the nearby small graben structure of site 2 (Fig. 9g). Complex seismogenic ruptures show approximately 50–100 m wide surface breaks with main faults, antithetic and secondary cracks along normal faults during large earthquakes such as the Borah Peak large event (*Ms* 7.3, 1983 in Idaho, Crone *et al.* 1988). Rotated sedimentary units in the hangingwall of an active fault illustrate a coseismic flexural deformation likely associated with an antithetic fault at depth. A similar faulting structure was observed in trenches excavated across the Wasatch normal fault at Kaysville where the bending of the hangingwall sedimentary units leans progressively toward the fault plane (Swan *et al.* 1980; Stephenson *et al.* 1993; McCalpin *et al.* 1994).

The Bruderholz scarp provides a surprisingly clear geomorphic signature for the BR fault over a distance of 8 km. This is a minimum observed length while the dislocation model of a fault capable to produce vertical coseismic displacements of 1 m may reach a Mw 6.7 and related intensity IX-X earthquakes (Kanamori & Anderson 1975; Ambraseys & Free 1997). This suggests that the fault likely extends to the north and/or to the south. The northern rim of the Bruderholz scarp is completely erased by the Rhine river and dense urbanization. However, early 1960s construction works along the BR

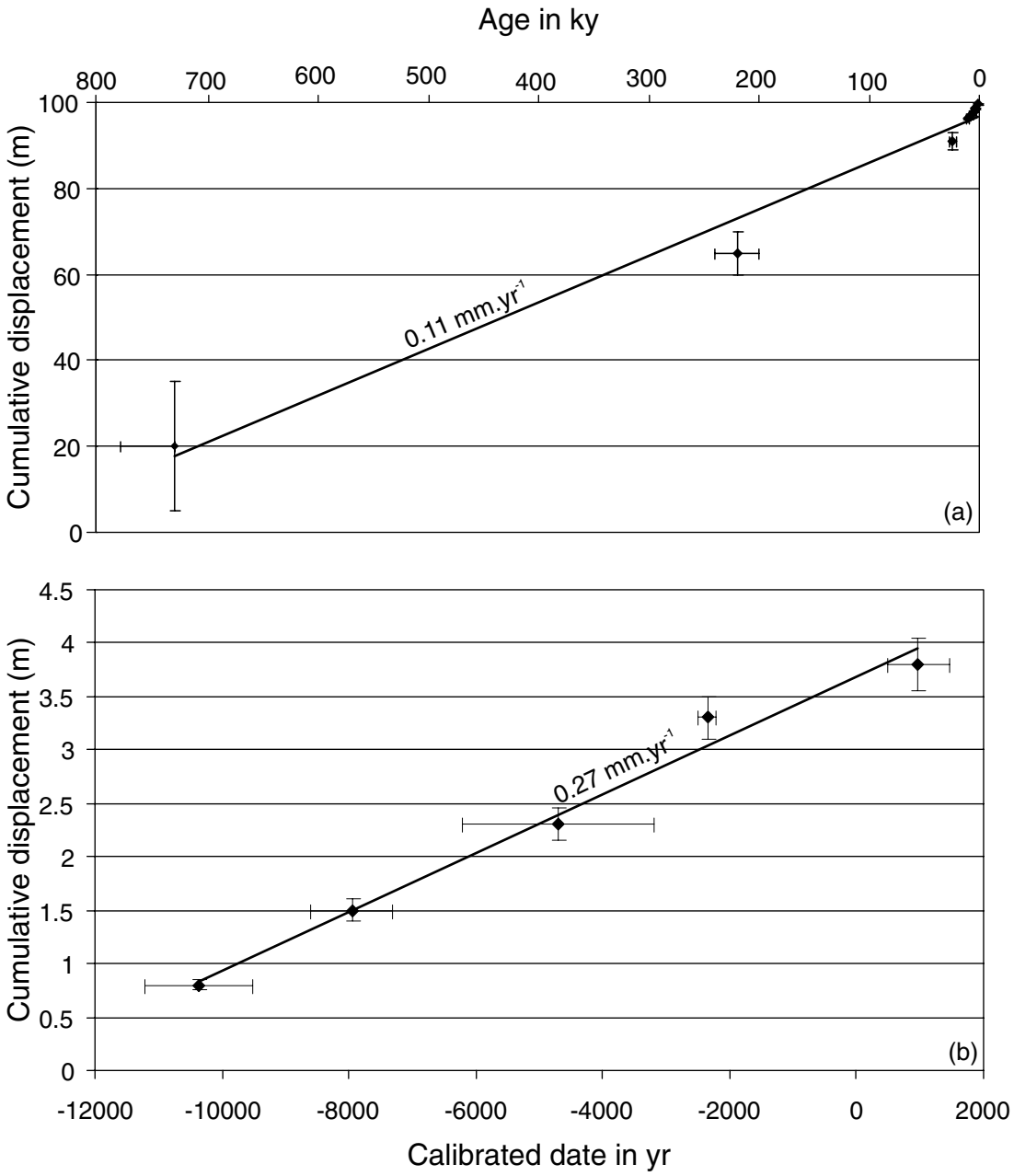

Figure 13. (a) Long-term uplift rate as determined from Quaternary alluvial terraces cropping out along the BR fault scarp. (b) Cumulative displacement as a function of time for the late Pleistocene and the Holocene along the Basel–Reinach (BR) fault. Inferred displacement rate of 0.27 mm yr^{-1} is in good agreement with previous results (Meghraoui *et al.* 2001). Trend line fits well data points with $R^2 > 0.98$.

fault in the southern suburbs of Basel (Barsch *et al.* 1971) exhibits evidence for late Pleistocene–Holocene faulting (Fig. 9e). Hence, a northern extension of the BR fault through the city of Basel is very likely. It may then connect to the Wiese valley, the similar morphology of which is mainly inherited from the Rhine valley flexure.

To the south, the BR fault does not display a noticeable morphology as it meets the frontal folds of the Jura mountains. The topographic signal of the Blauen fold (see Fig. 4) strongly overprints any component related to the fault. However, field investigations permitted us to find broken and faulted limestone units on the crest of the Blauen along the rigorously southern extension of the fault. Besides, the electrical tomography profile GE6 (see Fig. 8) exhibits resistivity contrasts the geometry of which suggests the presence of a major fault with more than 40 m (penetration depth) of vertical displacement at station 200 and two secondary recent faults at stations 250 and 300, which affect shallow sediments. Such a detectable vertical displacement indicates that site 3 is not the southern end of the BR fault, which probably extends partly through the Blauen.

At depth, the BR fault should intersect the regional Rhine valley flexure fault (RVFF) at a depth of 6 to 7 km. However, it is unlikely that the BR fault cuts through the RVFF and should rather be considered as a well-developed splay or antithetic fault. As we could

not evidence any sign of recent activity on the RVFF, we suggest that ruptures nucleate at depth, possibly close to the junction of the faults and propagate downwards along the RVFF and upwards along the BR fault as the upper section of the RVFF would be locked. Consequently, the border RVFF system is likely to be active and its activity documented along the BR fault.

8.2 Seismotectonic characteristics and deformation rate

If the best stress tensor found by the inversion of the regional focal mechanism (Plenefisch & Bonjer 1997) is applied to the BR fault, assuming that the fault dips 80° to the east, a normal component of motion is inferred but with a dominant left-lateral motion. Results from the geomorphological and palaeoseismological investigations point towards a dominant normal faulting component on the fault without excluding a strike-slip component.

This apparent contradiction may signify that the fault is not responding in a straightforward way to the regional stress tensor. Hence, the regional stress tensor obtained from small to moderate size earthquakes may not reflect very local stress conditions and the solution found by the inversion should be representative of the actual regional stress tensor. A possible explanation for the inconsistency may be that some left-lateral motion on the BR fault exists but has not been observed because our trenches are dug normal to the fault and because strike-slip offsets on slow faults are more easily erased by erosion than vertical offsets. Near-surface stress measurements (Becker 2000) indicate that the maximum horizontal stress displays smooth variations around an N–S direction over NE Switzerland. Nonetheless, it also points to a well-constrained strong heterogeneity marked by E–W measurements at the eastern edge of the Laufen basin (Fig. 3) located south of the Birs valley. If applied to the deeper crust, this could bias the representativity of the stress tensor inferred from focal mechanisms.

Plotting cumulative displacement as a function of time (Fig. 13) reveals a very constant vertical deformation rate of 0.27 mm yr^{-1} for the late Pleistocene and the Holocene in good agreement with previous works in the Rhine graben (Meghraoui *et al.* 2000, 2001). It is as well consistent with a recent study of the ITRF97 velocity field (Nocquet *et al.* 2001), which suggests active NW–SE extension of 1–1.5 mm yr^{-1} within the lower and upper Rhine graben structures. In their palaeoseismological analysis of the Bree fault, Meghraoui *et al.* (2001) inferred a mean vertical deformation rate of 0.07 mm yr^{-1} and a mean recurrence interval of ∼15 000 yr for the Bree fault. These parameters are similar to those determined for other stable continental regions (Bossu & Grasso 1996; Crone *et al.* 1997) but differ somehow from those of the BR fault. With a mean vertical deformation rate of 0.27 mm yr^{-1} and a mean recurrence interval of 2500 yr, the BR fault seems to display a faulting behavior similar to what has been observed along the Apennines ranges in Italy (Pantosti *et al.* 1993; D'Addezio *et al.* 2001).

8.3 Implications for the seismic hazard

In areas of slow faults and moderate seismicity, the historical record is too short to cover the cyclic recurrence of large earthquakes. Palaeoseismology may extend the historical record and provide a basis for a more realistic evaluation of the seismic hazard. Our objective is to achieve a probabilistic seismic hazard assessment to produce models of earthquake recurrence and subsequently estimate probability of ground shaking. We calibrate the earthquake recurrence model introducing the palaeoearthquake record of the BR fault.

Using the Earthquake Catalogue of Switzerland from AD 1300 (Fäh *et al.* 2003), declustered following the Reasenberg approach (Reasenberg 1985), we defined the Basel seismic source according to the polygon: 48.07°N°E, 48.05°N–8.01°E, 47.43°N–7.76°E and 47.45°N–7.35°E. In addition, we add the three most recent earthquakes for the past 7800 yr including the AD 1356 event, as observed on the Reinach fault palaeoseismic study ($Mw = 6.4$–6.7 from Meghraoui *et al.* 2001 and this study). According to the recent re-evaluation of the historical seismicity of Switzerland (Fäh *et al.* 2003), we assume that all of the three events have the same magnitude $Mw = 6.9 \pm 0.5$. The recurrence parameters are calculated using the maximum likelihood approach that incorporates the completeness periods (Bender 1983) and its ZMAP implementation (Wiemer 2001). We assess the fit of five models to the long-term and short-term seismicity in the Basel region (see M1–M5 in Fig. 14). The selection of the preferred model is based on the Akaike Information Criterion (AIC) score (Imoto 1991; Ogata 1999).

Models 4 and 5 obtain the best fit to the seismicity of the Basel region, as seen in Fig. 14. A key element is the single palaeoseismic point (3 events in 7800 yr). This point receives a high weight in the inversion as it provides a constraint over a long period of time. Our preferred *b* value (0.79) is significantly lower than the national 0.9 average and provides an overall good fit to the instrumental, historical and pre-historical seismicity. If only the historical record was available, we would obtain a *b* value of 0.68, resulting in an erroneous, too large contribution of large earthquakes in the assessment of seismic hazard. This is a consequence of the different return period for the 1356 event as estimated from the historical record and in the palaeoseismic record.

Finally, we perform a simplistic estimation of the annual strain rate in the Basel region for the best-fitting model, assuming that all earthquakes have the same focal mechanism, and adopting a Kostrov formulation (Kostrov 1974) with a 15 km thickness of the seismogenic layer. The annual deformation across the Basel area is displayed in Fig. 14 as a function of the assumed Mmax.For example, Mmax = 5.9 would result in an annual deformation of 0.1 mm, while Mmax = 7.2 results in a deformation rate of approximately 0.21 mm yr^{-1} (inset Fig. 14, dashed horizontal line). This estimate is derived using the best model in Fig. 14 and thus including the palaeoseismic data for the last 7800 yr.

ACKNOWLEDGMENTS

We are grateful to many earth scientists who visited the trenches and provided fruitful discussions. Walter Frey (Geoconsult) conducted high-resolution reflection seismics, Leibniz Labor (Kiel) and ETH Zurich radiocarbon datings and Quaternary TL Surveys TL datings. We thank the students and colleagues who helped with fieldwork, especially Peter Schürch, Ina Spottke and Hubert Mvondo and the technical team from IPG Strasbourg. We are grateful to Stefan Wiemer for his contribution to Fig. 14 and for discussion about earthquake recurrence. We thank the community of Reinach and the Bürgergemeinde of Reinach for providing access to properties and technical help in the field. Investigations along the BR scarp were funded by the SAFE project of the European Commission (EVG1-2000-22005), the Swiss Federal Institute of Technology (ETHZ), the Swiss National Fund and the HSK (Swiss Federal Nuclear Safety Inspectorate).

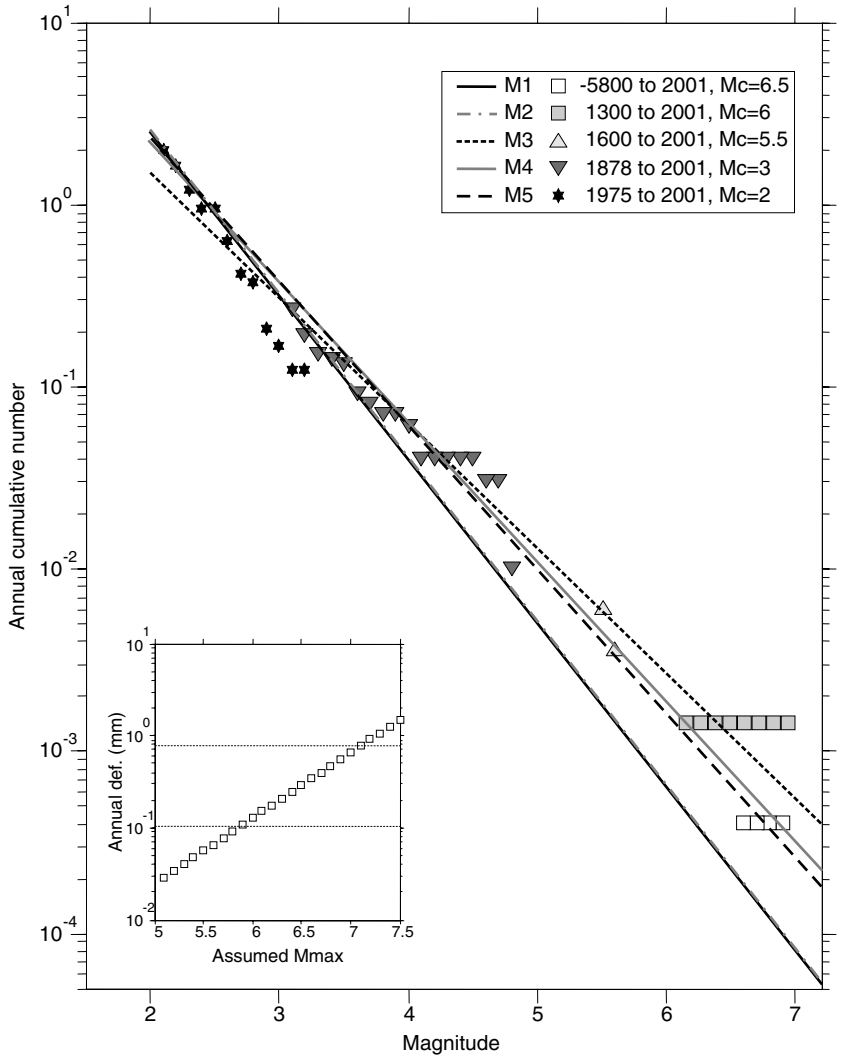

Figure 14. Cumulative annual rate of events as a function of magnitude for events in the Basel region. Symbols indicate five different completeness periods models: M1, fixed $b = 0.9$, variable a value (AIC: 66.505, a value = 2.2, b value 0.9, weight = 0.18); M2, fixed $b = 0.9$ and two variable a values, one for the instrumental data (1975–2001) and one for the historical period 1878–1975 (AIC: 68.487, a value = 2.22, b value = 0.9, weight = 0.068); M3, variable b value and two variable a values (AIC: 66.322, a value = 1.56, b value 0.69, weight = 0.2); M4, variable b and a values (AIC: 65.81, a value = 1.89, b value = 0.77, weight = 0.26); M5, Bayesian error weighted b value (the weight between 0 and 1 is determined proportional to the uncertainties and sample sizes of the two b values, AIC: 65.589, a value = 1.94, b value = 0.79, weight = 0.29). The small inset displays the annual strain rate in mm as a function of assumed Mmax, using a Kostrov model (Kostrov 1974) with a 15 km depth extend of the seismogenic zone. The annual rate of deformation is approximately 0.2 mm yr^{-1} on the basis of palaeoseismological data (Meghraoui *et al.* 2001) and approximately 0.8 mm yr^{-1} on the basis of historical data solely (Fäh *et al.* 2003).

REFERENCES

Ambraseys, N. & Free, M.W., 1997. Surface-wave magnitude calibration for European region earthquakes, *J. Earthquake Eng.,* **1**(1), 1–22.

Barsch, D., Hauber, L. & Schmid, E., 1971. Birs und Rhein bei St. Jakob (Basel) im Spätpleistozän und Holozän, *Regio Basiliensis,* **12**(2), 286–314.

Becker, A., 2000. The Jura Mountains–an active foreland fold-and-thrust belt?, *Tectonophysics,* **321,** 381–406.

Becker, A., Davenport, C.A. & Giardini, D., 2002. Palaeoseismicity studies on end-Pleistocene and Holocene lake deposits around Basle, Switzerland, *Geophys. J. Int.,* **149,** 659–678.

Bender, B., 1983. Maximum likelihood estimation of b-values for magnitude grouped data, *Bull. seism. Soc. Am.,* **73,** 831–851.

Bitterli-Brunner, P. & Fischer, H., 1988. *Erläuterungen zu Blatt 1067 Arlesheim des Geologischer Atlas der Schweiz 1:25'000,* Schweiz. Geol. Komm, Bern.

Bossu, R. & Grasso, J.R., 1996. Stress analysis in the intraplate area of Gazli, Uzbekistan, from different sets of earthquake focal mechanisms, *J. geophys. Res.,* B., **101**(8), 17 645–17 659.

Bronk Ramsey, C., 1995. Radiocarbon Calibration and Analysis of Stratigraphy: the OxCal Program, *Radiocarbon,* **37**(2), 425–430.

Camelbeeck, T. & Meghraoui, M., 1998. Geological and geophysical evidence for large paleoearthquakes with surface faulting in the Roer Graben (northwest Europe), *Geophys. J. Int.,* **132,** 347–362.

Camelbeeck, T., Alexandre, P., Vanneste, K. & Meghraoui, M., 2000. Long-term seismicity in regions of present day low seismicity: the example of western Europe, *Soil Dyn. Earth. Eng.,* **20,** 405–414.

Crone, A.J., Machette, M.N., Bonilla, M.G., Lienkaemper, J.J., Pierce, K.L., Scott, W.E. & Bucknam, R.C., 1988. Surface faulting accompanying the Borah Peak earthquake and segmentation of the Lost River fault, central Idaho, *Bull. seism. Soc. Am.,* **77**(3), 739–770.

Crone, A.J., Machette, M.N. & Bowman, J.R., 1997. Episodic nature of earthquake activity in stable continental regions revealed by

paleoseismicity studies of Australian and North American Quaternary faults, *Aust. J. Earth Sci.,* **44,** 203–214.

D'Addezio, G., Masana, E. & Pantosti, D., 2001. The Holocene paleoseismicity of the Aremogna-Cinque Miglia Fault (Central Italy), *J. Seism.,* **5,** 181–205.

Doebel, F. & Olbrecht, W., 1974. An Isobath Map of the Tertiary Base in the Rhinegraben, in *Approaches to Taphrogenesis,* pp. 71–72, eds Illies, J.H. & Fuchs, K. , Schweizerbart, Stuttgart.

Fäh, D. *et al.,* 2003. Earthquake Catalogue Of Switzerland (ECOS) and the related macroseismic database, *Eclogae geol. Helv.,* **96,** 219–236.

Fujimoto, K., Tanaka, H., Tomida, N., Ohtani, T. & Ito, H., 2000. Characterization of fault gouge from GSJ Hirabayashi Core samples and implications for the activity of the Nojima Fault. In: *Proc. International workshop on the Nojima Fault core and borehole data analysis*, USGS Open-file report 00-0129,103–109, United States Geological Society, Washington, DC.

Gürler, B., Hauber, L. & Schwander, M., 1987. *Die Geologie der Umgebung von Basel mit Hinweisen über die Nutzungsmöglichkeiten der Erdwärme,* Schweiz. Geol. Komm., Bern.

Haas, J.N., Richoz, I., Tinner, W. & Wick, L., 1998. Synchronous Holocene climatic oscillations recorded on the Swiss plateau and at timberline in the alps, *Holocene,* **8**(3), 301–309.

Imoto, M., 1991. Changes in the Magnitude Frequency B-Value Prior to Large (M- Greater-Than-or-Equal-to-6.0) Earthquakes in Japan, *Tectonophysics,* **193**(4), 311–325.

Johnston, A.C., 1996. Seismic moment assessment of earthquakes in stable continental regions: I, Instrumental seismicity, *Geophys. J. Int.,* **124**(2), 381–414.

Kanamori, H. & Anderson, D.L., 1975. Theoretical basis of some empirical relations in seismology, *Bull. seism. Soc. Am.,* **65**(5), 1073–1095.

Kostrov, B.V., 1974. Seismic moment and energy of earthquakes and seismic flow of rock, *Izv. Acad. Sci. USSR Phys. Solid Earth,* **1,** 23–44.

Lambert, J., 1997. Les tremblements de terre en France, hier, aujourd'hui, demain, *Editions BRGM*, Orleans.

Laubscher, H., 2001. Plate interactions at the southern end of the Rhine graben, *Tectonophysics,* **343,** 1–19.

Lemeille, F., Cushing, M., Carbon, D., Grellet, B., Bitterli, T., Flehoc, C. & Innocent, C., 1999. Co-seismic ruptures and deformations recorded by speleothems in the epicentral zone of the Basel earthquake, *Geodin. Acta,* **12**(3–4), 179–191.

McCalpin, J.P., 1996. *Paleoseismology*, Academic Press, San Diego.

McCalpin, J.P., Forman, S.L. & Lowe, M., 1994. Reevaluation of Holocene faulting at the Kaysville site, Weber segment of the Wasatch fault zone, Utah, *Tectonics,* **13**(1), 1–16.

Magny, M., Guiot, J. & Schoellamer, P., 2001. Quantitative reconstruction of Younger Dryas to mid-Holocene paleoclimates at Le Locles, Swiss Jura, using pollen and lake-level data, *Quat. Res.,* **56,** 170–180.

Mayer-Rosa, D. & Cadiot, B., 1979. A review of the 1356 Basel earthquake : basic data, *Tectonophysics,* **53,** 325–333.

Meghraoui, M., Camelbeeck, T., Vanneste, K., Brondeel, M. & Jongmans, D., 2000. Active faulting and paleoseismology along the Bree fault, lower Rhine graben, Belgium, *J. geophys. Res.,* **105,** 13 809–13 841.

Meghraoui, M., Delouis, B., Ferry, M., Giardini, D., Huggenberger, P., Spottke, I. & Granet, M., 2001. Active normal faulting in the upper Rhine graben and paleoseismic identification of the 1356 Basel earthquake, *Science,* **293,** 2070–2073.

Meschede, M., Asprion, U. & Reicherter, K., 1997. Visualization of tectonic structures in shallow-depth high-resolution ground-penetrating radar (GPR) profiles, *TerraNova,* **9,** 167–170.

Meyer, B., Lacassin, R., Brulhet, J. & Mouroux, B., 1994. The Basel 1356 earthquake : which fault produced it?, *TerraNova,* **6,** 54–63.

Montandon, F., 1943. Les séismes de forte intensité en Suisse, *Rev. Etude Calamités (Union Intern. Secours, B.),* **5**(18–19), 107–169.

Nivière, B. & Winter, T., 2000. Pleistocene northwards fold propagation of the Jura within the southern Upper Rhine Graben: seismotectonic implications, *Global and Planet. Change,* **27,** 263–288.

Nocquet, J.-M., Calais, E., Altamimi, Z., Sillard, P. P., & Boucher, C., 2001. Intraplate deformation in western Europe deduced from an analysis of the International Terrestrial Reference Frame 1997 (ITRF97) velocity field, *J. geophys. Res.,* **106**(B6), 11 239–11 257.

Ogata, Y., 1999. Seismicity analysis through point-process modeling: A review, *Pure appl. Geophys.,* **155**(2–4), 471–507.

Orellana, N., 2002. Mécanismes de déformation et contrôle structural des failles de Bâle (Fossé Rhénan) et Pygarki (Fossé de Corinthe), in *Mémoire de D.E.A.*, Université Louis Pasteur, Strasbourg.

Pantosti, D., Schwartz, D. & Valensise, G., 1993. Paleoseismology along the 1980 surface rupture of the Irpinia Fault; implications for earthquake recurrence in the Southern Apennines, Italy, *J. geophys. Res.,* **98**(4), 6561–6577.

Plenefisch, T. & Bonjer, K.-P., 1997. The stress field in the Rhine Graben area inferred from earthquake focal mechanisms and estimation of frictional parameters, *Tectonophysics,* **275,** 71–97.

Reasenberg, P.A., 1985. Second-order moment of Central California Seismicity, *J. geophys. Res.,* **90,** 5479–5495.

Schleicher, M., Grootes, P.M., Nadeau, M.-J. & Schoon, A., 1998. The carbonate ^{14}C background and its component at the Leibniz AMS facility, *Radiocarbon,* **40**(1), 85–93.

Stephenson, W.J., Smith, D.G. & Pelton, J.R., 1993. A high-resolution seismic reflection and gravity survey of Quaternary deformation across the Wasatch fault, Utah, *J. geophys. Res.,* **98**(B5), 8211–8223.

Stuiver, M. *et al.,* 1998. INTCAL98 Radiocarbon Age Calibration, 24000-0 cal BP, *Radiocarbon,* **40**(3), 1041–1083.

Suzuki, K., Toda, S., Kusunoki, K., Fujimitsu, Y., Mogi, T. & Jomori, A., 2000. Case studies of electrical and electromagnetic methods applied to mapping active faults beneath the thick quaternary, *Eng. Geol.,* **56,** 29–45.

Swan, F.H., Schwartz, D.P. & Cluff, L.S., 1980. Recurrence of moderate to large magnitude earthquakes produced by surface faulting on the Wasatch fault zone, Utah, *Bull. seism. Soc. Am.,* **70**(5), 1431–1462.

Vanneste, K., Verbeeck, K., Camelbeeck, T., Paulissen, E., Meghraoui, M., Renardy, F., Jongmans, D. & Frechen, M., 2001. Surface-rupturing history of the Bree fault scarp, Roer Valley graben: Evidence for six events since the late Pleistocene, *J. Seism.,* **5,** 329–359.

Vogt, J., 1979. Les tremblements de terre en France, *Mem. Bur. Rech. Geol. Min.,* **96,** 153–165.

Wallace, R.E., 1977. Profiles and ages of young fault scarps, North-central Nevada, *Bull. geol. Soc. Am.,* **88**(9), 1267–1282.

Wells, D.L. & Coppersmith, K.J., 1994. New empirical relationships among magnitude, rupture length, rupture width, rupture area, and surface displacement, *Bull. seism. Soc. Am.,* **84**(4), 974–1002.

Wiemer, S., 2001. A software package to analyze seismicity: ZMAP, *Seism. Res. Lett.,* **72,** 373–382.

Zollinger, G., 1991. Zur Landschaftsgenese und Quartärstratigraphie am südlichen Oberrheingraben–am Beispiel der Lössdeckschichten der Ziegelei in Allschwil (Kanton Basel-Landschaft), *Eclogae geol. Helv.,* **84**(3), 739–752.

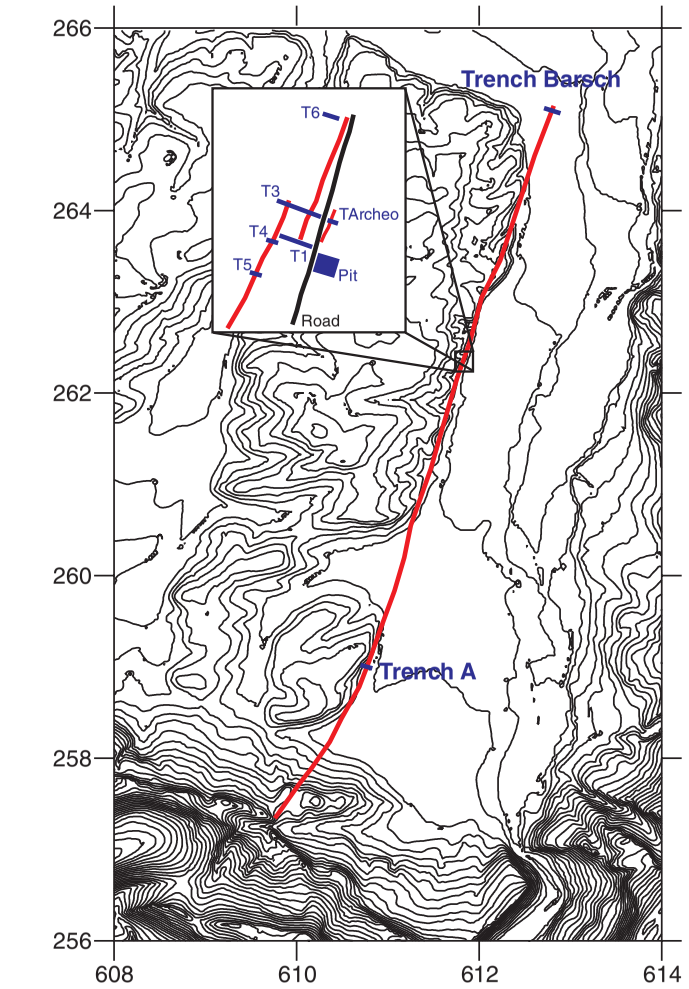

(a)

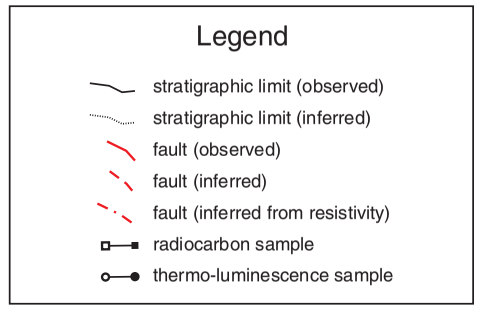

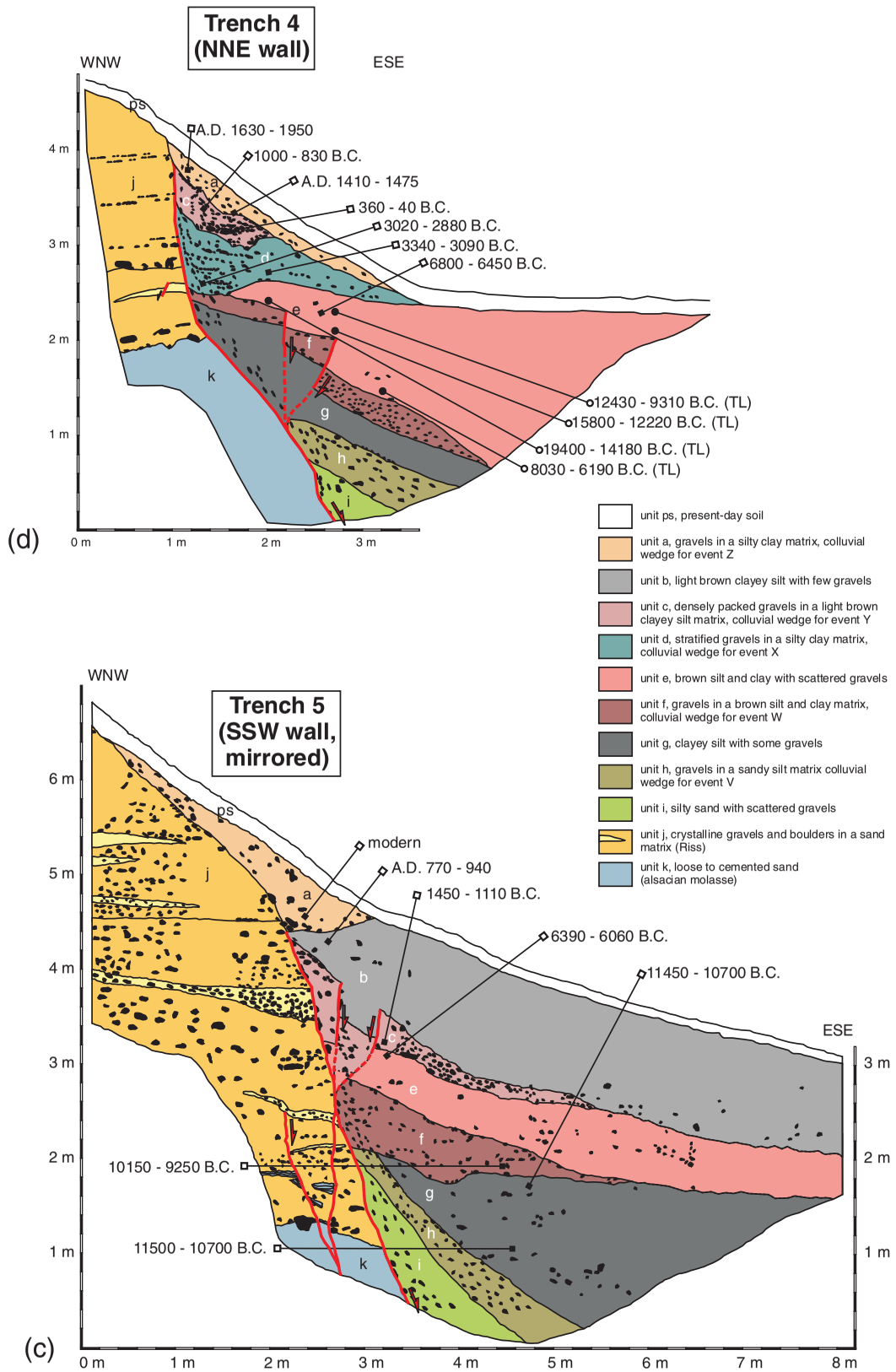

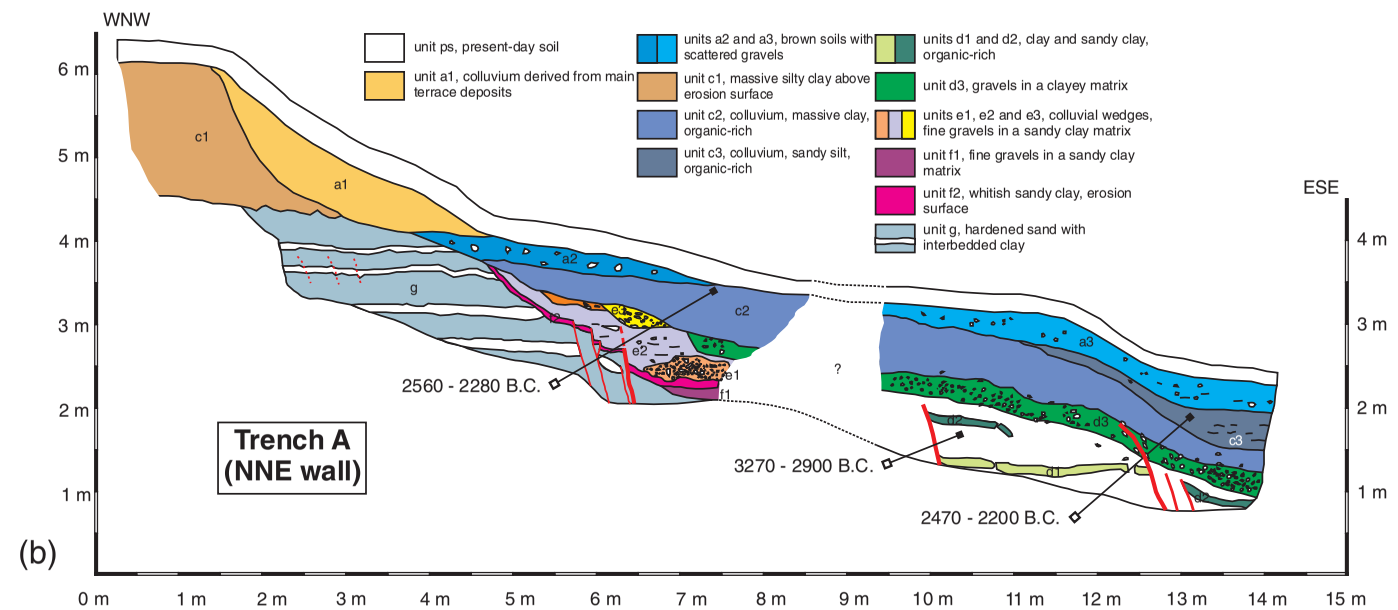

(b)

(c)

Figure 9. (a) Location map of detailed logs obtained from trench excavations during this study. (b), (c), (d), (f) and (g) Trench logs with unit descriptions and age determinations from radiocarbon and thermoluminescence (TL) data (see text and dating information Tables 2 and 4 for details). (e) Re-interpreted log of a construction trench opened in Basel and originally described by Barsch *et al.* (1971).

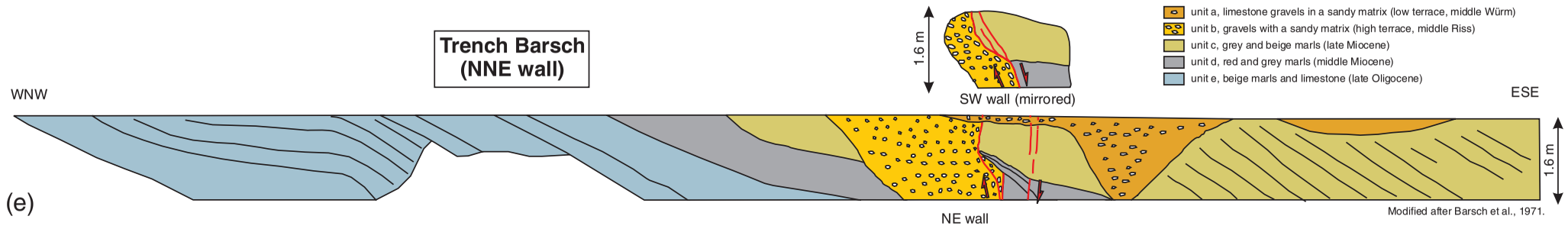

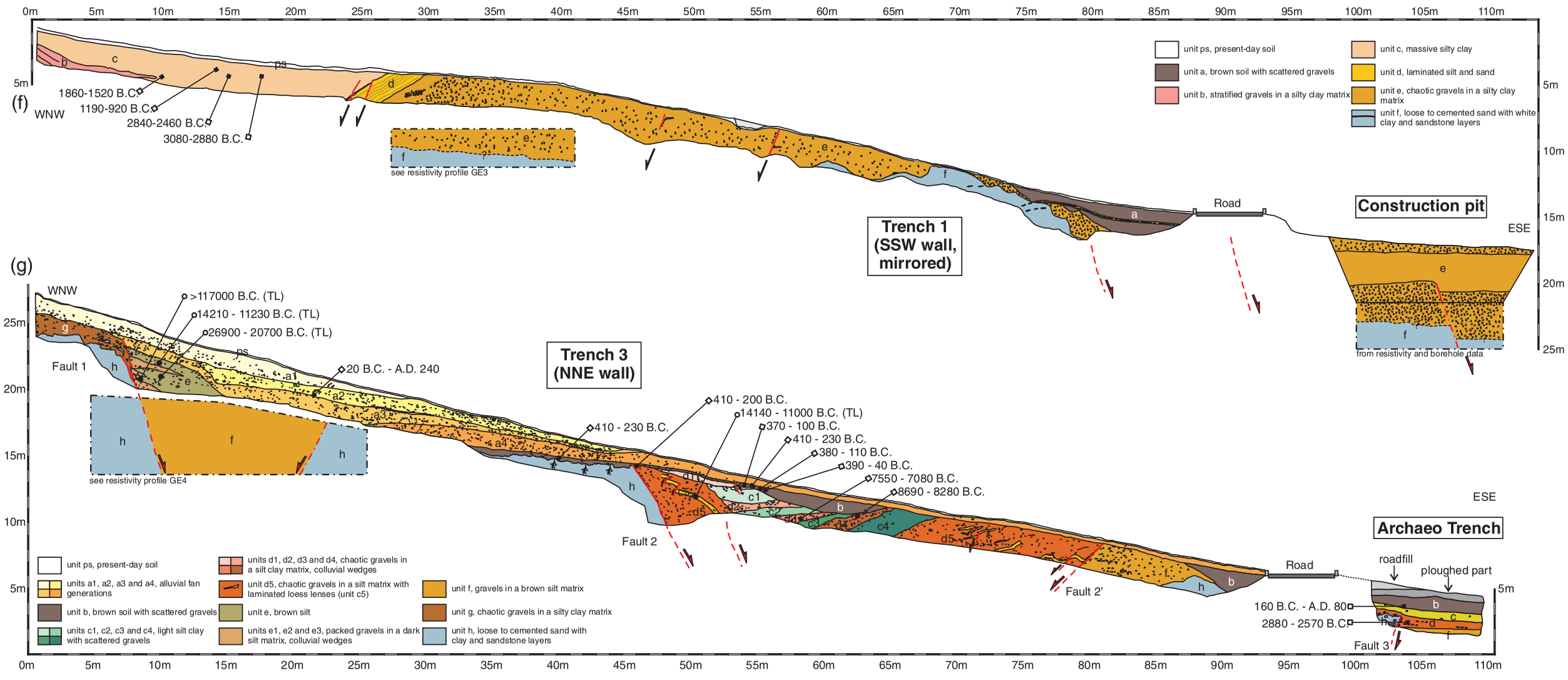

Figure 9. (*Continued.*)